ELSEVIER

Ocean Modelling 37 (2002) 55–88

Ocean Modelling

www.elsevier.com/locate/omodol

An oceanic general circulation model framed in hybrid isopycnic-Cartesian coordinates

Rainer Bleck *

Atmospheric and Climate Science, Los Alamos National Laboratory, MS B296 EES-8, Los Alamos, NM 87545, USA

Received 12 June 2001; received in revised form 23 July 2001; accepted 23 July 2001

Abstract

A newly developed hybrid-coordinate ocean circulation model is documented and tested. Coordinate surfaces in this model adhere to isopycnals wherever this does not violate minimum layer thickness requirements; elsewhere, coordinate surfaces are geometrically constrained. The intent of this approach, some of whose features are reminiscent of the Arbitrary Lagrangian–Eulerian (ALE) technique, is to combine the best features of isopycnic-coordinate and fixed-grid circulation models within a single framework. The hybrid model is an offshoot of the Miami Isopycnic Coordinate Ocean Model whose solutions, obtained under identical geographic and forcing conditions, serve as reference. Century-scale simulations on a coarse-mesh near-global domain show considerable similarities in the modeled thermohaline-forced circulation. Certain architectural details, such as the choice of prognostic thermodynamic variables (ρ, S versus T, S) and the algorithm for moving coordinate surfaces toward their reference isopycnals, are found to only have a minor impact on the solution. Emphasis in this article is on the numerical resiliency of the hybrid coordinate approach. Exploitation of the model's flexible coordinate layout in areas of ocean physics where pure isopycnic coordinate models only have limited options, such as mixed-layer turbulence parameterization, will be the subject of forthcoming articles.

1. Introduction

Faithful replication of the conservation properties inherent in the laws of physics is a near-universal goal in numerical modeling. In the case of rotating, stratified geophysical flows, the conservation properties of the equations comprised in a particular model can be manipulated not only by changing the size of the computational mesh or the sophistication of the operators

* Tel.: +1-505-665-9150; fax: +1-505-667-5921.
E-mail address: bleck@lanl.gov (R. Bleck).

1463-5003/02/$ - see front matter
PII: S1463-5003(01)00012-9

Report Documentation Page

Form Approved
OMB No. 0704-0188

1. REPORT DATE	2. REPORT TYPE	3. DATES COVERED
JUL 2001		**00-00-2001 to 00-00-2001**

4. TITLE AND SUBTITLE	5a. CONTRACT NUMBER
An oceanic general circulation model framed in hybrid isopycnic-Cartesian coordinates	5b. GRANT NUMBER
	5c. PROGRAM ELEMENT NUMBER
6. AUTHOR(S)	5d. PROJECT NUMBER
	5e. TASK NUMBER
	5f. WORK UNIT NUMBER
7. PERFORMING ORGANIZATION NAME(S) AND ADDRESS(ES) **Los Alamos National Laboratory,Atmospheric and Climate Science,MS B296 EES-8,Los Alamos,NM,87545**	8. PERFORMING ORGANIZATION REPORT NUMBER
9. SPONSORING/MONITORING AGENCY NAME(S) AND ADDRESS(ES)	10. SPONSOR/MONITOR'S ACRONYM(S)
	11. SPONSOR/MONITOR'S REPORT NUMBER(S)

12. DISTRIBUTION/AVAILABILITY STATEMENT
Approved for public release; distribution unlimited

13. SUPPLEMENTARY NOTES

14. ABSTRACT

15. SUBJECT TERMS

16. SECURITY CLASSIFICATION OF:			17. LIMITATION OF ABSTRACT	18. NUMBER OF PAGES	19a. NAME OF RESPONSIBLE PERSON
a. REPORT **unclassified**	b. ABSTRACT **unclassified**	c. THIS PAGE **unclassified**	**Same as Report (SAR)**	**34**	

mimicking spatial and temporal differentiation, but also by transforming the conservation laws from a Cartesian to a nonCartesian vertical coordinate. The latter manipulation explains the multitude of vertical coordinates proposed over the years for use in atmospheric and oceanic circulation models.

Perhaps the most striking example of such manipulation of the governing equations is the use of entropy as vertical coordinate (Montgomery, 1937; Starr, 1945). This transformation – made possible in the oceanic context by the fact that entropy (or its proxy, potential density ρ_{pot}) varies monotonically with depth in most parts of the world ocean – reduces the First Law of Thermodynamics in the important case of adiabatic flow to the simple statement $\dot{\rho}_{\text{pot}} \equiv \mathrm{d}\rho_{\text{pot}}/\mathrm{d}t = 0$. This in turn renders adiabatic fluid motion two-dimensional in $(x, y, \rho_{\text{pot}})$ space. These simplifications readily carry over to the algebraically approximated equations in numerical models using entropy as vertical coordinate.

Fluid mixing and stirring likewise are handled more concisely if carried out in ρ_{pot} space where a sharp line can be drawn between eddy-driven isopycnal stirring and diapycnal mixing. Both processes are important in the ocean but typically act on vastly different space and time scales.

One particular incarnation of fluid laws formulated in $(x, y, \rho_{\text{pot}})$ space is the so-called stacked shallow water model, a system of equations describing the dynamics of a stratified fluid in terms of the dynamics of a set of interacting constant-potential density layers. Stacked shallow water models have been widely used as theoretical tools elucidating aspects of large-scale oceanic and atmospheric flow (example: baroclinic instability). Use of this paradigm in numerical models also has a long history, at least in process models dealing with particular aspects of fluid behavior. On the other hand, full-fledged oceanic circulation models built upon the use of entropy as vertical coordinate have been developed only quite recently (Bleck et al., 1992; Oberhuber, 1993).

The tradeoffs between advantages and disadvantages of isopycnal modeling (the word isopycnal refers here to the property $\rho_{\text{pot}} = \text{const.}$) have been the subject of vigorous debate. While there is little disagreement about the potential advantages, the discomfort about the disadvantages of isopycnal modeling varies greatly among numerical practitioners. The most serious drawbacks of an entropy-based vertical coordinate are its degeneracy in unstratified and statically unstable water columns and, to a lesser extent, the possibility that coordinate surfaces intersect the sea surface or bottom. While robust numerical methods have been developed to deal with the latter aspect, the prevailing opinion in the community is that modeling of oceanic flow in unstratified – let alone convectively unstable – regions cannot properly be done in potential density space.

Another, more practical drawback of isopycnal modeling is the requirement that the vertical grid in an isopycnic model span a wide enough range to capture the extremes of water density found anywhere in modeled domain. Many grid points in density space are thereby "wasted". To put it differently: The world ocean does not fit snugly into a rectangular box in (x, y, ρ) space.

This paper presents initial results obtained with a numerical model which, while still primarily an isopycnic coordinate model, addresses all of the above concerns by allowing coordinate surfaces to deviate locally from isopycnals wherever the latter either fold, outcrop, or generally provide inadequate vertical resolution in portions of the modeled domain.

The concept of "hybrid" coordinates that act in the above-described manner is not new. The groundwork for formulating the equations governing geophysical fluid flow in a generalized vertical coordinate was laid by Starr (1945), Kasahara (1974), and Bleck (1978a). Coordinate

surfaces that adhere to isopycnals, except in regions where these outcrop, were introduced two decades ago by Bleck and Boudra (1981) (hereafter BB81) in a study of the wind-driven circulation in an idealized ocean basin. The rationale for the use of hybrid coordinates at that time, at least from the perspective of the BB81 authors, was lack of numerical skill in dealing with the outcrop problem. Hence, the hybrid coordinate concept was promptly shelved when techniques for numerically solving the shallow-water equations in the limit of zero layer thickness became available (e.g., Bleck, 1984; Bleck and Boudra, 1986). Elsewhere, however, hybrid ocean modeling continued (Zebiak and Cane, 1987; Schopf and Loughe, 1995).

The BB81/Schopf hybridization approach differs from other generalized coordinate schemes developed over the years (e.g., Bleck, 1978b, and references therein; Zhu et al., 1992; Konor and Arakawa, 1997) in that it does away with an analytic formula specifying where in a fluid column a given grid point is located. Rather, the BB81/Schopf scheme assigns each grid point a reference or "target" isopycnal and continually tries to move individual grid points that have become separated from their target isopycnal back toward it. As grid points vertically migrate toward their target, they are subjected to repelling forces from grid points above or below. This device keeps grid points in a column from fusing. A "pure" isopycnic model may be viewed as a hybrid model in which the repelling force is set to zero.

While hybrid coordinates – hybrid in the narrow BB81 sense – lost some of their appeal in ocean modeling with the arrival of robust methods for handling fused grid points, i.e., massless coordinate layers, the idea gained acceptance in meteorology. A hybrid-isentropic weather prediction model based on the BB81 concept (Bleck and Benjamin, 1993) has been in use by the US Weather Service since the mid-1990s under the acronym Rapid Update Cycle (RUC).

From today's perspective, adoption of hybrid coordinates in isopycnic ocean modeling is necessitated not so much by the outcropping problem but by the degeneracy of isopycnic coordinate representation in unstratified or convectively unstable water columns. In this paper we discuss some early results obtained with a hybrid model which is an outgrowth of MICOM, the Miami Isopycnic Coordinate Ocean Model (Bleck et al., 1992). Emphasis in this paper is on a fairly thorough documentation of model numerics; hence, there is no room here for an exhaustive discussion of model results. Given that the present model is not only designed for specialized process studies but also for comprehensive tasks such as climate prediction, emphasis in Section 5 will be on aspects of the modeled thermohaline-driven circulation.

2. Model overview

In this section, the salient features of the new hybrid model will be described. The model will be referred to as HYCOM, the hybrid coordinate version of MICOM.

2.1. Governing equations

HYCOM, like MICOM, is a primitive-equation model containing 5 prognostic equations – two for the horizontal velocity components, a mass continuity or layer thickness tendency equation, and two conservation equations for a pair of thermodynamic variables, such as salt and

temperature or salt and density. The model equations, written in (x, y, s) coordinates, where s is an unspecified vertical coordinate, are

$$\frac{\partial \mathbf{v}}{\partial t_s} + \nabla_s \frac{\mathbf{v}^2}{2} + (\zeta + f)\mathbf{k} \times \mathbf{v} + \left(\dot{s}\frac{\partial p}{\partial s}\right)\frac{\partial \mathbf{v}}{\partial p} + \nabla_s M - p\nabla_s \alpha = -g\frac{\partial \boldsymbol{\tau}}{\partial p} + \left(\frac{\partial p}{\partial s}\right)^{-1} \nabla_s \cdot \left(\nu \frac{\partial p}{\partial s}\nabla_s \mathbf{v}\right), \tag{1}$$

$$\frac{\partial}{\partial t_s}\left(\frac{\partial p}{\partial s}\right) + \nabla_s \cdot \left(\mathbf{v}\frac{\partial p}{\partial s}\right) + \frac{\partial}{\partial s}\left(\dot{s}\frac{\partial p}{\partial s}\right) = 0, \tag{2}$$

$$\frac{\partial}{\partial t_s}\left(\frac{\partial p}{\partial s}\theta\right) + \nabla_s \cdot \left(\mathbf{v}\frac{\partial p}{\partial s}\theta\right) + \frac{\partial}{\partial s}\left(\dot{s}\frac{\partial p}{\partial s}\theta\right) = \nabla_s \cdot \left(\nu \frac{\partial p}{\partial s}\nabla_s \theta\right) + \mathscr{H}_\theta, \tag{3}$$

where $\mathbf{v} = (u, v)$ is the horizontal velocity vector, p is pressure, θ represents any one of the model's thermodynamic variables, $\alpha = \rho_{\text{pot}}^{-1}$ is the potential specific volume, $\zeta \equiv \partial v/\partial x_s - \partial u/\partial y_s$ is the relative vorticity, $M \equiv gz + p\alpha$ is the Montgomery potential, $gz \equiv \phi$ is the geopotential, f is the Coriolis parameter, $\mathbf{k}$ is the vertical unit vector, ν is a variable eddy viscosity/diffusivity coefficient, and $\boldsymbol{\tau}$ is the wind- and/or bottom-drag induced shear stress vector. $\mathscr{H}_\theta$ represents the sum of diabatic source terms, including diapycnal mixing, acting on θ. Subscripts indicate which variable is held constant during partial differentiation. Distances in x, y direction, as well as their time derivatives $\dot{x} \equiv u$ and $\dot{y} \equiv v$, are measured in the projection onto a horizontal plane. This convention renders the coordinate system nonorthogonal in 3-D space but eliminates metric terms related to the slope of the s surface (Bleck, 1978a).

Other metric terms, created when vector products involving $(\nabla\cdot)$ or $(\nabla\times)$ are evaluated on a nonCartesian grid (e.g., in spherical coordinates), are absorbed into the primary terms by evaluating vorticity and horizontal flux divergences in (1)–(3) as line integrals around individual grid boxes. Note that applying ∇ to a scalar, such as $\mathbf{v}^2/2$ in (1), does not give rise to metric terms.

After vertical integration over a coordinate layer bounded by two surfaces $s_{\text{top}}, s_{\text{bot}}$ (the ocean surface, the sea floor, and all interior layer interfaces are s surfaces in this context), the continuity equation (2) becomes a prognostic equation for the layer weight per unit area, $\Delta p = p_{\text{bot}} - p_{\text{top}}$:

$$\frac{\partial}{\partial t_s}\Delta p + \nabla_s \cdot (\mathbf{v}\Delta p) + \left(\dot{s}\frac{\partial p}{\partial s}\right)_{\text{bot}} - \left(\dot{s}\frac{\partial p}{\partial s}\right)_{\text{top}} = 0. \tag{4}$$

The expression $(\dot{s}\partial p/\partial s)$ represents the vertical mass flux across an s surface, taken to be positive if in $+p$ (downward) direction.

Multiplication of (1) by $\partial p/\partial s$ and integration over the interval $(s_{\text{top}}, s_{\text{bot}})$, followed by division by $\Delta p/\Delta s$, changes the shear stress term in that equation into

$$\frac{g}{\Delta p}(\boldsymbol{\tau}_{\text{top}} - \boldsymbol{\tau}_{\text{bot}})$$

while the lateral momentum mixing term integrates to

$$(\Delta p)^{-1}\nabla_s \cdot (\nu \Delta p \nabla_s \mathbf{v}). \tag{5}$$

All other terms in (1) retain their formal appearance.

Wind-induced and bottom stresses are prorated among coordinate layers in accordance with the assumption that they vary linearly over a prescribed finite depth range typically chosen to be of order 10 m.

The layer-integrated form of (3) is

$$\frac{\partial}{\partial t}\theta\Delta p + \nabla_s \cdot (\mathbf{v}\theta\Delta p) + \left(\dot{s}\frac{\partial p}{\partial s}\theta\right)_{\text{bot}} - \left(\dot{s}\frac{\partial p}{\partial s}\theta\right)_{\text{top}} = \nabla_s \cdot (\nu\Delta p\nabla_s\theta) + \mathscr{H}_\theta. \tag{6}$$

The above prognostic equations are complemented by several diagnostic equations, including

- the hydrostatic equation

$$\frac{\partial M}{\partial \alpha} = p, \tag{7}$$

- an equation of state linking potential temperature T, salinity S, and pressure p to $\alpha^{-1} = \rho_{\text{pot}}$, and
- an equation prescribing the vertical mass flux $(\dot{s}\partial p/\partial s)$ through an s surface.

The last-mentioned equation controls both spacing and movement of layer interfaces and thus comprises the essence of hybrid coordinate modeling; we refer to the algorithm built around this equation as the "grid generator", to be described in detail in Section 3.

The horizontal pressure gradient term $(\nabla_s M - p\nabla_s\alpha = \alpha\nabla_z p)$ in (1) must be formulated so as to properly transmit interface pressure torques up and down the water column. (Not adhering to this principle would, for example, cause the model to violate the Sverdrup relation between wind stress curl and meridional barotropic flow.) The scheme developed for this purpose is discussed in Appendix A.

The use of *potential* specific volume in (7) and in the definition of M can be justified by arguments similar to those given in Sun et al. (1999, Section 4b).

2.2. Transport and mixing processes

Owing to the fact that coordinate layers in HYCOM are predominantly isopycnic, the model in its present implementation shares with MICOM several algorithms for handling transport and mixing in 3-D model space.

The prognostic equations are time-integrated using the split–explicit treatment of barotropic and baroclinic modes developed for MICOM (Bleck and Smith, 1990, hereafter BS90). The split–explicit approach, while fraught with numerical stability problems (Higdon and Bennett, 1997), has proven to be advantageous for executing ocean models on massively parallel computers because it does not require solution of an elliptic equation.

2.2.1. Horizontal transport and mixing

Following MICOM tradition, horizontal mass fluxes are computed using the Flux Corrected Transport scheme (Zalesak, 1979) while horizontal tracer transport, which in a model featuring variable vertical mesh spacing must be done in flux form, is handled by a variant of the MPDATA scheme described by Drange and Bleck (1997). The Coriolis and horizontal momentum advection terms combined [terms 2 and 3 in (1)] are evaluated in potential-enstrophy conserving form. To achieve this, the finite-difference analog of the term $(\zeta + f)\mathbf{k} \times \mathbf{v}$ must be written as an analog of

$((\zeta + f)/\Delta p)\mathbf{k} \times (\mathbf{v}\Delta p)$. The method developed for handling a vanishing denominator ($\Delta p = 0$) is described in Appendix B of BS90.

In contrast to recent MICOM versions where, for the sake of computational efficiency, the constraint $\rho_{\text{pot}} = \text{const.}$ is used to reduce the number of thermodynamic prognostic variables from two to one in interior layers, HYCOM carries two prognostic thermodynamic variables everywhere. (The prognostic variable used in MICOM is salinity. Temperature is computed by inverting the equation of state which for this purpose is approximated by a third degree polynomial in T (Brydon et al., 1999).)

Intralayer subgridscale turbulent mass redistribution, often referred to as bolus transport, is implemented in both models via layer interface smoothing. This scheme is conceptually identical to the Gent and McWilliams (1990) mixing scheme, except that it is used here in its underlying isopycnal form. Since interface smoothing has no effect in regions where coordinate surfaces are geometrically constrained, the bolus transport parameterization in HYCOM is only active in the isopycnic part of model space. This restriction is unlikely to have adverse effects on model dynamics as long as nonisopycnic coordinate layers are essentially confined to the surface mixed layer.

The interface smoothing term in MICOMs continuity equation was originally formulated as a Laplace operator, meaning that interface displacement was set proportional to the Laplacian $\nabla^2 p$ of interface pressure p. Several years ago, a switch was made to biharmonic smoothing where interface displacement is set proportional to $-\nabla^4 p$. This change was prompted by concerns that Laplacian interface smoothing may have a systematic shoaling effect on layer interfaces, considering the bowl shape of isopycnals in the vertical-meridional plane.

The biharmonic smoothing concept is retained in HYCOM.

2.2.2. Surface mixed layer

The assured presence of nicely spaced coordinate layers in the uppermost part of the water column allows formulation of turbulent near-surface mixing in terms of, for example, K theory. For reasons of computational economy and model-to-model continuity, the HYCOM version discussed here retains a Kraus and Turner (1967) slab mixed layer.

The Kraus–Turner (KT hereafter) closure scheme is particularly well-suited to models that treat the mixed layer bottom as a coordinate surface. This is the case in MICOM but certainly not in the present model. Attempts to suppress the diffusive effect of the spatial mismatch between model interfaces and the mixed layer bottom – mainly by splitting the coordinate layer bracketing the mixed layer base into two sublayers – were altogether unsuccessful. The KT implementation chosen for the present suite of experiments therefore makes no effort in this direction, nor does it keep a record of the depth of the physical mixed layer base or the density contrast across it from one time step to the next. Rather, it treats the ad hoc stairstep density profile defined by the discrete model layers at any instant as "reality" and operates on it accordingly. (Note that so-called layer models typically treat coordinate layers as vertically homogeneous; hence, properties such as temperature and salinity are piecewise constant in the vertical but exhibit zero-order discontinuities at layer interfaces.)

The KT closure scheme operates in one of two modes depending on the sign of the surface buoyancy flux. A buoyancy flux that stabilizes the water column acts as a drain on near-surface turbulence kinetic energy (TKE). In this case, the mixed layer depth is determined by the ratio of

the TKE-producing wind stress and the TKE-draining buoyancy flux, that is, by the Monin–Obukhov length. If the buoyancy flux destabilizes the water column, the KT scheme stipulates that the TKE generated jointly by wind stress and buoyancy loss is converted to potential energy by entraining into the mixed layer an appropriate amount of denser water from below. In the first case, knowledge of the mixed layer depth at the beginning of a given model time step is not required, but in the second case the outcome of the entrainment calculation does depend on this quantity.

This is where the present KT implementation sacrifices accuracy for simplicity's sake. Starting at the top of the water column, the program looks for the first "stairstep" in the density profile and defines the interface where this happens as the mixed layer base. A possible concern is the ill-posedness introduced by the fact that infinitesimal changes in layer density may lead to potentially large changes in the mixed layer base estimate. Fortunately, this ill-posedness is inconsequential in the context of the KT scheme because the potential energy gained by entraining water of density $\rho + \epsilon$ into a layer of density ρ approaches zero as ϵ goes to zero. This is to say that the outcome of the entrainment calculation is not overly sensitive to misdiagnosing the initial mixed layer base.

Once the mixed layer depth at the end of a given model time step has been determined, the water column is homogenized down to that depth. The resulting T/S profile is then projected back onto the model coordinate layers which maintain their thickness throughout the process. This last step, which is not found in MICOM, generally causes water mass properties to be exchanged across the mixed layer base. It makes the KT mixed layer in the present model inherently more diffusive than in MICOM and calls into question the fidelity of the KT scheme in coarse-vertical resolution models unless they treat – as MICOM does – the mixed layer base as a layer interface. In an attempt to counteract this diffusion, the TKE generation term in the present suite of experiments has been artificially reduced by 50%.

2.2.3. Interior diapycnal mixing

MICOM uses the diapycnal mixing algorithm of McDougall and Dewar (1998) which is tailored to layer models treating density as piecewise constant in the vertical. Since the latter is also true in HYCOM, the Dewar–McDougall scheme is carried over without modification.

In the HYCOM version discussed here, the diapycnal mixing equations are solved explicitly in time. Numerical stability constraints in this case do not allow mixing coefficients of the size typically found in turbulent flow regions. Newer versions of HYCOM are available which, by solving the relevant equations implicitly (Hallberg, 2000), maintain numerical stability and thus enable the model to use K theory to mix fluid throughout the water column regardless of whether the flow is turbulent or laminar. Both mixed layer closure and patchy turbulence in sill overflows stand to benefit from this treatment.

2.2.4. Deep convection

MICOM maintains stable stratification in each grid column by absorbing into the mixed layer any mass-containing interior layer whose density falls below the mixed layer density. This type of mixed-layer entrainment, akin to convective adjustment, is independent of entrainment resulting from TKE closure. It plays a vital role in creating ultra-deep "mixed layers" which the model needs to form and detrain abyssal water masses.

HYCOM, likewise, resorts to convective adjustment to maintain stable stratification. However, since density in this model is not guaranteed to increase with depth in layers below the surface layer, convective adjustment must be allowed to take place between any two adjoining model layers. As in fixed-grid models, interface depths remain unchanged in HYCOM while homogenization of the pair of statically unstable layers takes place.

2.3. Sea ice model

A simple sea ice model is used is to handle the energetic consequences of water phase changes in polar regions. The model, which has much in common with one developed by Semtner (1976, Appendix) focuses on three (and only three) aspects, namely the prevention of water temperatures below the freezing point, the effect of freezing and melting on mixed-layer salinity, and the impact of the ice surface on ocean-atmosphere energy fluxes.

If outgoing surface heat fluxes cause the mixed layer temperature at a given location to drop below the freezing point of -1.8 °C, the ice model extends a repayable "energy loan" to the mixed layer at this location to maintain a -1.8 °C temperature. The loan amount obviously is proportional to the amount of liquid water converted to ice. If the surface heat flux is directed so as to supply heat to the ocean, any outstanding energy loan balance at a given location must be repaid (i.e., the existing ice must be melted) before SST is allowed to rise above -1.8 °C.

Salinity fluxes though the ice-water interface that result from melting and freezing of ice are computed based on the assumption that ice contains 25 g/kg less salt than sea water.

Sea ice profoundly affects surface energy fluxes, both by virtue of its high albedo compared to water and because an ice surface can be much colder than open water. The approach taken to compute heat fluxes across the upper and lower surfaces of the ice sheet is described in Appendix B.

3. The grid generator

Here we describe an experimental scheme that allows coordinate layers to maintain finite thickness, at the price of becoming nonisopycnic, wherever lack of stratification would cause isopycnic layers to collapse to zero thickness. [1] The resulting hybrid coordinate system puts isopycnic grid points which in a "pure" isopycnic model are deactivated (i.e., fused to others at the sea surface or the bottom of the slab mixed layer) to use in improving vertical model resolution.

An important point to note is that layer inflation only takes place in the upper ocean; no efforts are made to inflate massless coordinate layers fused to the sea floor. Doing so would create steeply inclined nonisopycnic coordinate layers in places like the shelf break which would introduce a class of numerical problems familiar from scaled-depth ("σ") coordinate [2] models (Janjic, 1977).

[1] Both MICOM and HYCOM sidestep the Boussinesq approximation by using pressure p in lieu of height z as the "geometric" vertical coordinate. Accordingly, terms like Cartesian, thickness, depth, etc., refer to p rather than z.

[2] The letter σ has three different meanings in this paper: sea water density anomaly, pressure divided by bottom pressure, and Stefan–Boltzmann constant.

MICOMs technique for handling the intersection of isopycnals with topography, documented in detail in Appendix A of BS90, has withstood the test of time (e.g., Smith, 1992) and has been retained in HYCOM.

Aside from maintaining minimum layer thickness in the upper part of the water column, the grid generator is also in charge of restoring isopycnic conditions in coordinate layers wherever possible. The biggest challenge in this regard is the annual buildup and obliteration of the seasonal thermocline. Warming and cooling of the ocean from above creates coordinate layers in HYCOM that are isopycnal in character during summer but change into geometrically defined layers in winter. Considerable freedom exists in placing the latter in the water column. Since seasonal heating/cooling creates/destroys isopycnals right at the surface, a strategy allowing geometrically defined layers to stay near the surface during winter minimizes seasonal grid migration and concomitant dispersion of water mass properties. On the other hand, allowing them to descend to greater depths in winter improves vertical grid spacing in deep mixed layers and prevents "data voids" that may cause the model to misrepresent springtime mode water formation. The scheme decribed here sacrifices uniform vertical resolution in the mixed layer for the sake of minimizing nonmaterial interface migration during spring and fall.

The scheme, outlined in greater detail in Appendix C, is designed to be highly local for computational simplicity's sake. Not only does it operate in one dimension – the vertical –, but it determines the need for moving gridpoints ("regridding") by considering the properties of only three adjoining coordinate layers. It begins by checking the density in a particular layer against its target value. If a discrepancy is found, only one interface is moved, resulting in mass exchange with either the layer above or below.

Conceptually the simplest way of reducing/increasing water density in a given layer is by diluting the layer with water from above/below. This approach is akin to upstream or donor cell advection of mass in the vertical, and as such it has rather benign (though diffusive) numerical properties. It also has the potential disadvantage of always causing layers whose density is off target to *grow* at the expense of neighboring layers.

An alternative approach, this one retaining the flavor of centered advection schemes, is (i) to divide the layer whose density we wish to modify into two sublayers of different densities, and (ii) to expel one sublayer. For this scheme to yield the desired result, one sublayer density must be chosen to correspond to the desired target density, while the density of the other sublayer should match the density (actual or target) of the layer above or below, as the case may be.

While it may sound physically implausible that the density in a layer can be manipulated by extruding water into an adjacent layer, this operation is legitimate as long as it does not create new extrema in temperature or salinity. For this reason, the "unmixing" process just described must remain confined to a "bounding box" in T/S space whose four sides are defined in terms of the T/S values in the given layer and its two neighbors. See Appendix C for numerical details.

The unmixing ("UX") approach just described differs from the diluting ("DL") approach described earlier in that it causes layers whose density is off target to *shrink*. Having two schemes available allows us to design composite regridding schemes. Given that in many situations the T/S bounding box constraint will prevent formation of sublayers having the appropriate densities, it is necessary to follow the UX step, if employed at all, by a DL step.

The effect of the vertical transport terms on the prognostic variables in (4) and (6) is a by-product of the regridding process just described. Vertical momentum transport is evaluated

separately, using an upstream (donor cell) scheme and the mass flux ($\dot{s}\partial p/\partial s$) implied by regridding.

The hybrid grid treatment described here may be viewed as a special 1-D case of the Arbitrary Lagrangian–Eulerian (ALE) scheme introduced by Hirt et al. (1974). It differs from common applications of the ALE scheme in one important aspect, namely, the emphasis placed here on regridding for the sake of restoring isopycnal conditions in coordinate layers, in addition to regridding for the sake of maintaining minimum grid point spacing.

4. Experimental setup

HYCOMs performance will be demonstrated here by a series of 100-year simulations carried out on a near-global domain extending from 69°S to 65°N with a horizontal mesh size of $1.4° \times 1.4° \cos(latitude)$. Water depth is based on ETOPO5 data, averaged over individual grid squares but otherwise unsmoothed.

The vertical structure of the ocean is represented by 14 layers whose target densities are given in Table 1. Results will be compared with those from MICOM configured for the same domain and same 14 layers. (MICOMs top layer is a variable-density mixed layer, but coordinate values for the isopycnal layers match values 2–14 from Table 1.) Thermobaric effects on water density (Sun et al., 1999) are incorporated. The diapycnal mixing coefficient is set to $(2 \times 10^{-7}\ \mathrm{m^2\ s^{-2}})/N$ where N is the buoyancy frequency. Isopycnal diffusivity and viscosity values, including the one used for thickness diffusion (interface smoothing), are formulated as $u_d \Delta x$ where Δx is the local horizontal mesh size and u_d is of order 0.01 m s^{-1}. In regions of large shear, isopycnal viscosity is set proportional to the product of mesh-size squared and total deformation (Smagorinsky, 1963), the proportionality factor being 0.2.

Surface forcing is based on monthly climatologies of the following fields:

- surface air temperature, relative humidity, and rms wind speed from COADS (Woodruff et al., 1987);
- wind stress components from the European Centre for Medium-Range Weather Forecasting;
- net radiation from Oberhuber (1988) atlas;
- precipitation based on satellite microwave measurements (Spencer, 1993).

Instantaneous forcing values are obtained from the monthly fields using quasi-Hermite interpolation in time.

Annually averaged runoff from 14 major rivers totaling 0.43 Sv is added as point sources to the precipitation field at the appropriate river outflow locations. Another 0.27 Sv of freshwater input representing Antarctic ice melt is distributed uniformly along the southern domain boundary.

Table 1
Target densities ($\sigma_2 = \rho_{pot} - 1000$ kg m^{-3}) of the 14 model layers

k	1	2	3	4	5	6	7
σ_2	31.85	33.22	34.26	35.04	35.62	36.05	36.37
k	8	9	10	11	12	13	14
σ_2	36.61	36.79	36.92	37.01	37.07	37.11	37.14

Except for wind stress, the omission of freshwater input along the northern boundary, and the absence of imposed diapycnal fluxes mimicking the effect of bottom water formation in polar basins outside the computational domain, the above forcing fields agree with those used in previous near-global MICOM simulations (e.g., Bleck, 1998).

5. Results

We begin by showing in Fig. 1 an example of HYCOMs coordinate layer structure in relation to the density field. The feature to note is the approximate alignment of coordinate layers and isopycnals in the stratified portion of the ocean and, in contrast to this, their tendency to uncouple near the surface where coordinate layers flatten out while isopycnals rise to the sea surface. (Density is actually piecewise constant in the vertical within a coordinate layer, so some artistic license has been taken in generating this plot. The apparent density inversions in the transition zone between the isopycnal and constant-depth coordinate domains, as well as instances of obvious misalignment of the two sets of curves in the deep ocean, are caused by the vertical spline fitting scheme employed. In other words, in locations where layer interfaces and density isopleths appear to be only approximately aligned, they are actually perfectly aligned in the model.)

Fig. 1 illustrates two additional points: (i) the thickness of the top layer is held constant, except in very shallow water where interfaces are compressed in σ coordinate fashion, and (ii) no attempt is presently made to widen the vertical spacing of coordinate layers in unstratified parts of the

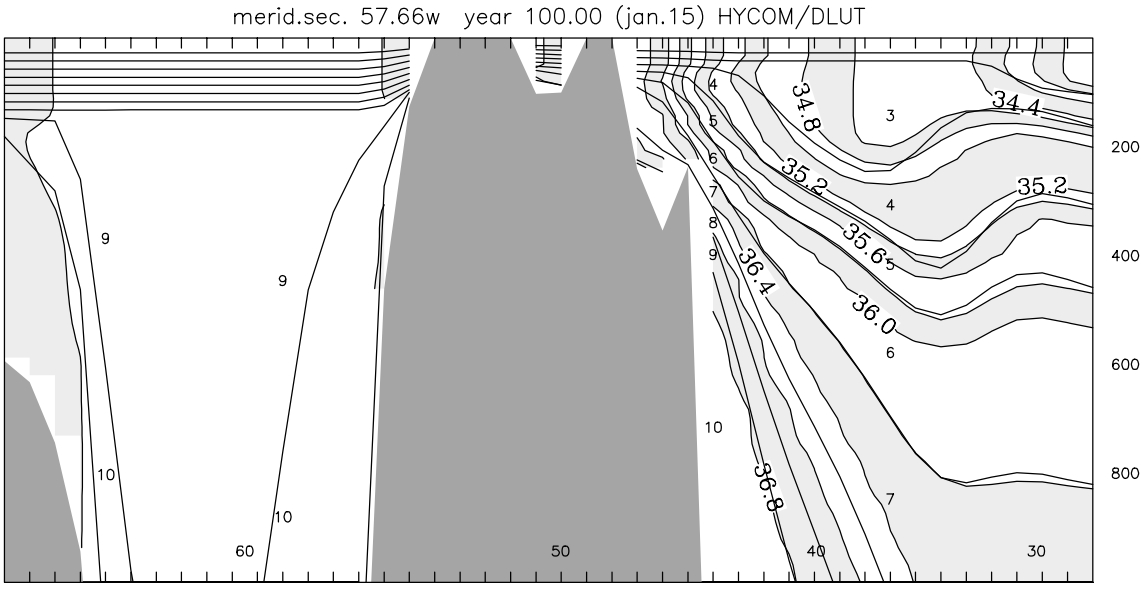

Fig. 1. Vertical section through upper 1000 m of DL solution at 57.7°W. Shaded contours: density anomaly (σ_2 units). Solid lines: coordinate surfaces. Small numbers: layer indices. Depth marked at right, latitude along bottom.

ocean, such as the Labrador Sea shown on the left. One reason for adhering to minimal spacing regardless of ambient stratification was mentioned in Section 3. Another reason is discussed in Appendix C.

Inspection of numerous cross-sections of the type shown in Fig. 1 has failed to reveal any signs of layer structure deterioration during the 100-year integration period. Specifically, the present grid generator shows no tendency to "coarsen" the steps in the density profile by, for example, deflating alternate coordinate layers. Note that there are no a-priori safeguards in the present grid generator that would prevent degeneracies and hysteresis effects of various kinds in the placement of isopycnal layers in the water column. The fact that the model is capable of maintaining a physically consistent layer structure over long periods, though difficult to document, is perhaps our most significant finding.

As mentioned earlier, two coordinate maintenance or grid generator schemes, named DL and UX, are being compared. The DL scheme modifies the density in a layer by diluting it with water from an adjacent layer, while the UX scheme resorts to unmixing, i.e., the formation of two sublayers of different densities and subsequent ejection of one sublayer, to modify the density in a given layer.

In addition, two versions of HYCOM are compared, one solving the prognostic equation (3) for potential temperature T and salinity S, and one solving (3) for potential density ρ_{pot} and S. The two model versions will be referred to as TS and RHO, respectively. While the eddy mixing term on the right-hand side of (3) is incorrect if ρ_{pot} replaces T as dependent variable, treating the pair ρ_{pot}, S as prognostic variables greatly simplifies the task of the grid generator whose actions are governed by the vertical distribution of ρ_{pot} rather than T or S. As pointed out in Appendix C, coordinate maintenance in the case of spatially varying T, S is inexact as the amount of mass transferred among layers is determined from the ρ_{pot} profile while the properties actually transferred are T and S.

The TS and RHO versions of HYCOM combined with the DL and UX grid generator options create a total of four model variants. Space restrictions only permit presentation of a few key results from the four model runs.

A relevant question to ask is which of the HYCOM versions tested comes closest to MICOM in preserving – or modifying, as the case may be – the oceanic density structure. To give an impression of the 100-year drift in the MICOM run itself, we show in Fig. 2 the contrast between zonally averaged interface depths at year 1 and year 100. The model drift indicated in the figure – rising interfaces (cooling) at thermocline depths combined with interface sinking (warming) in the abyssal ocean – is typical of century-scale simulations in which the diapycnal mixing coefficient is set inversely proportional to the buoyancy frequency. Insufficient Antarctic bottom water production clearly aggravates the density drift in this particular model run.

In assessing the diffusive properties of HYCOM one needs to keep in mind that coordinate maintenance leads to nonzero vertical transport terms [the terms involving $\dot{s}$ in (1)–(6)], and that one of the grid generators evaluates these terms using the notoriously diffusive upstream or donor cell scheme. Hence, we may expect the RHO version of HYCOM, in which coordinate maintenance invoked by density drift due to cabbeling does not occur, to be less diffusive than the TS version, at least in the deep ocean. Furthermore, the UX grid generator scheme can be expected to be less diffusive than the DL scheme, because the concept of "restoration by dilution" itself has a

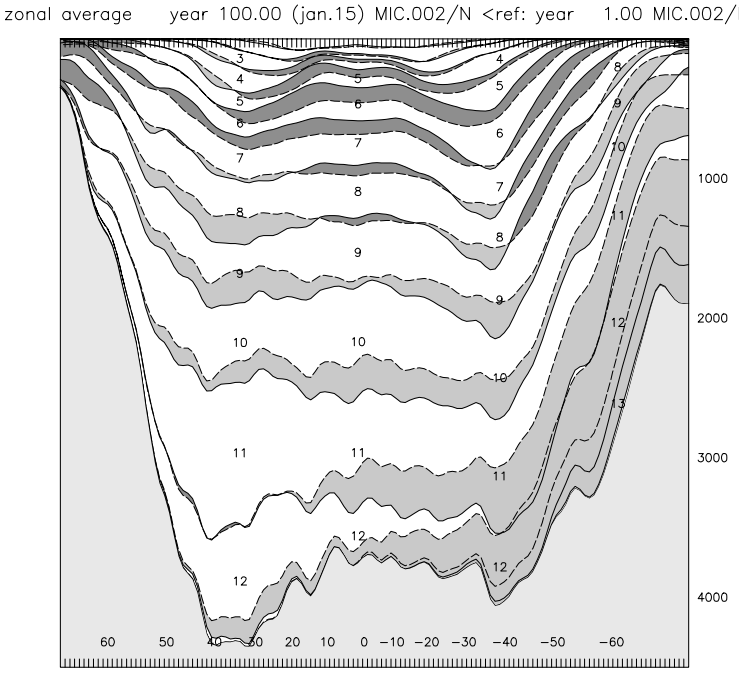

Fig. 2. Vertical–meridional section showing zonally averaged layer interface depths in MICOM at year 100. Light/dark shading indicates downward/upward interface displacement relative to interface position at year 1. Depth marked at right, latitude along bottom.

strong donor cell flavor whereas the concept of ''restoration by unmixing'' does not. In summary, the TS/DL combination should be the most diffusive one while the RHO/UX combination should be least diffusive.

The above expectations turn out to be true. To illustrate this, we show in Figs. 3 and 4 the zonally averaged vertical density structure at year 100 from the two runs showing the most extreme behavior, TS/DL and RHO/UX, referenced to the MICOM density field at year 100. To make this comparison meaningful, both MICOM and HYCOM results have been converted to potential density space by a coordinate transform method outlined in Appendix D. In the case of MICOM, this transformation boils down to apportioning the nonisopycnic uppermost model layer among the isopycnic ones.

Figs. 3 and 4 indicate warming in most parts of the basin compared to the MICOM run, but the warming is noticeably stronger in the TS/DL run than the RHO/UX run. In both HYCOM versions, the incremental drift appears to be comparable in magnitude to the drift seen in MICOM itself. We interpret this as an indication that none of the four coordinate maintenance schemes tested does inordinate damage to the oceanic density structure.

The 100-year integration period is long enough to allow for a significant deterioration of the thermohaline-forced meridional overturning circulation (MOC) in an ocean model. To investigate this aspect of model performance, we plot in Fig. 5 stream functions of the zonally integrated MOC from the MICOM run in the three major ocean basins and the world ocean as a whole,

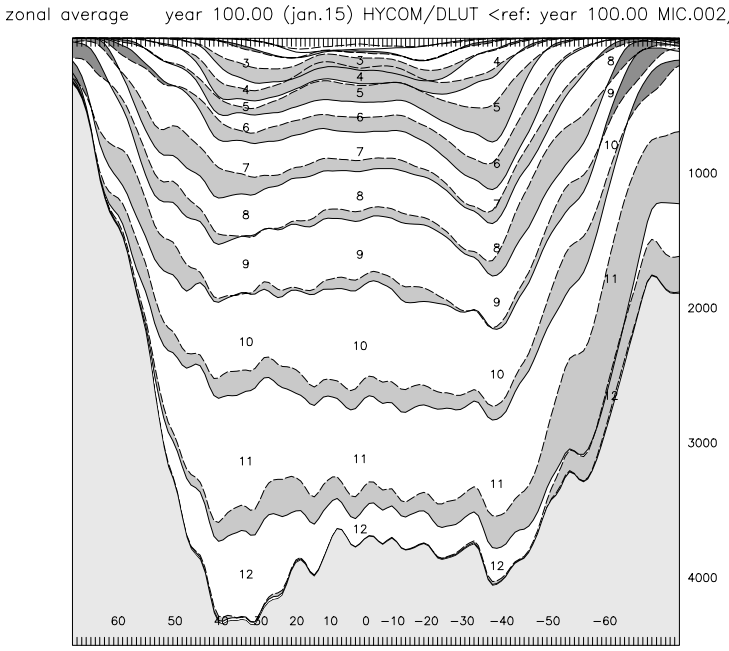

Fig. 3. Vertical–meridional section showing zonally averaged layer interface depths in TS/DL run at year 100. Light/dark shading indicates downward/upward interface displacement relative to MICOM reference solution. Depth marked at right, latitude along bottom.

averaged over model years 100–110. Fig. 6 shows the corresponding results from the HYCOM version that has just been shown to deviate most strongly from MICOM, namely, the TS/DL version.

The time-integrated mass fluxes, on which the overturning stream functions are based, were transformed from hybrid to ρ_{pot} space, using once again the scheme presented in Appendix D. The apparent compression of the streamfunction isopleths along the upper edge in the Pacific and Global panels could have been avoided by widening the range of output densities in the coordinate transform. Unfortunately, since the transform is done online, i.e., during formation of the time integral, repairing this defect would have required repeating all model runs.

Several features in Figs. 5 and 6 are in at least qualitative agreement with observational estimates of the MOC in the various parts of the world ocean (e.g., Schmitz, 1996a,b). Significant amounts of deep water are formed both in the North Atlantic and the Southern Ocean while the Pacific MOC shows relatively shallow cells driven by equatorial upwelling. The overturning cell driven by sinking in the North Atlantic extends far into the southern hemisphere. As already mentioned while discussing Fig. 2, far too little Antarctic Bottom Water is produced in the present model runs, and the small amount formed is not able to penetrate the northern hemisphere as observed.

The northern-hemispheric meridional heat flux is seen to be significantly higher in TS/DL (Fig. 6) than MICOM (Fig. 5). In the Atlantic, one reason for this difference is the behavior

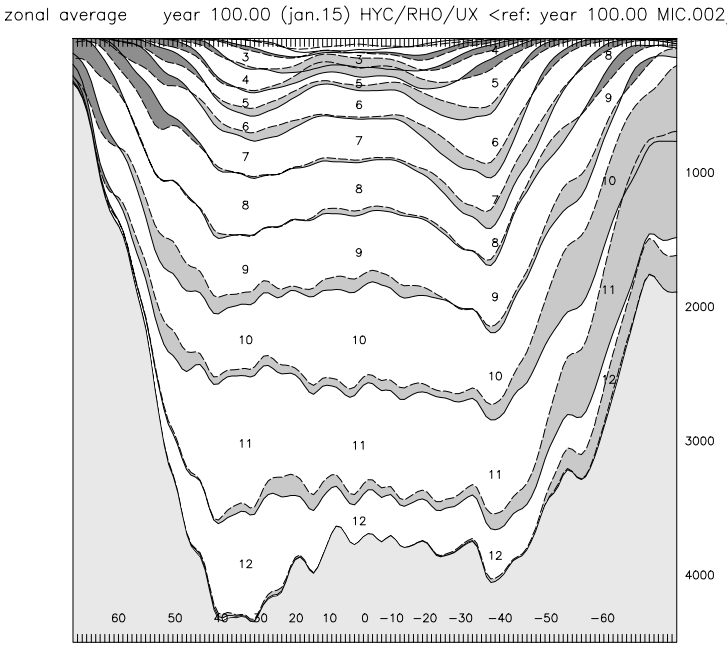

Fig. 4. As in Fig. 3, but for RHO/UX run.

of the North Atlantic Drift Current in the two models. Fig. 7 indicates that the NADC in HYCOM takes a more northerly path compared to MICOM, lowering the surface density south of Greenland by as much as 0.55 kg m^{-3}. The corresponding temperature increase (not shown) is as high as 3 °C, leading to a marked additional heat loss to the atmosphere. No explanation is offered at this time for the discrepancy regarding NADC positioning.

One of MICOMs traditional strengths is its ability to cleanly delineate geographic regions where the conversion of surface water to deep water takes place. It is of interest to investigate whether and to what extent HYCOM retains this advantage. The following results are based on methods developed by Sun and Bleck (2000) for quantitatively diagnosing 3-D mass fluxes in $(x, y, \rho_{\text{pot}})$ space. The assertion to be tested is that the RHO version of HYCOM does a better job than the TS version in delineating the downward branch of the MOC. As before, we use the MICOM solution as reference and base the discussion on model output transformed to ρ_{pot} space and averaged over model years 100–110.

Fig. 8 shows that MICOM injects roughly 9 Sv of water into isopycnal layer 12 (and possibly beyond) in the Labrador Sea, but rather insignificant amounts elsewhere in the North Atlantic. It is worth pointing out that that these diapycnal fluxes are far too large to result from interior diapycnal mixing; rather, they are caused by water mass transformation in the surface mixed layer which reaches into isopycnal layer 12 during at least part of the year.

The corresponding field from the TS/DL experiment is displayed in Fig. 9. The string of up- and downwelling cells along the Gulf Stream extension axis is the item of concern. As anticipated, these centers are largely eliminated if ρ_{pot}, S replace T, S as prognostic thermodynamic variables

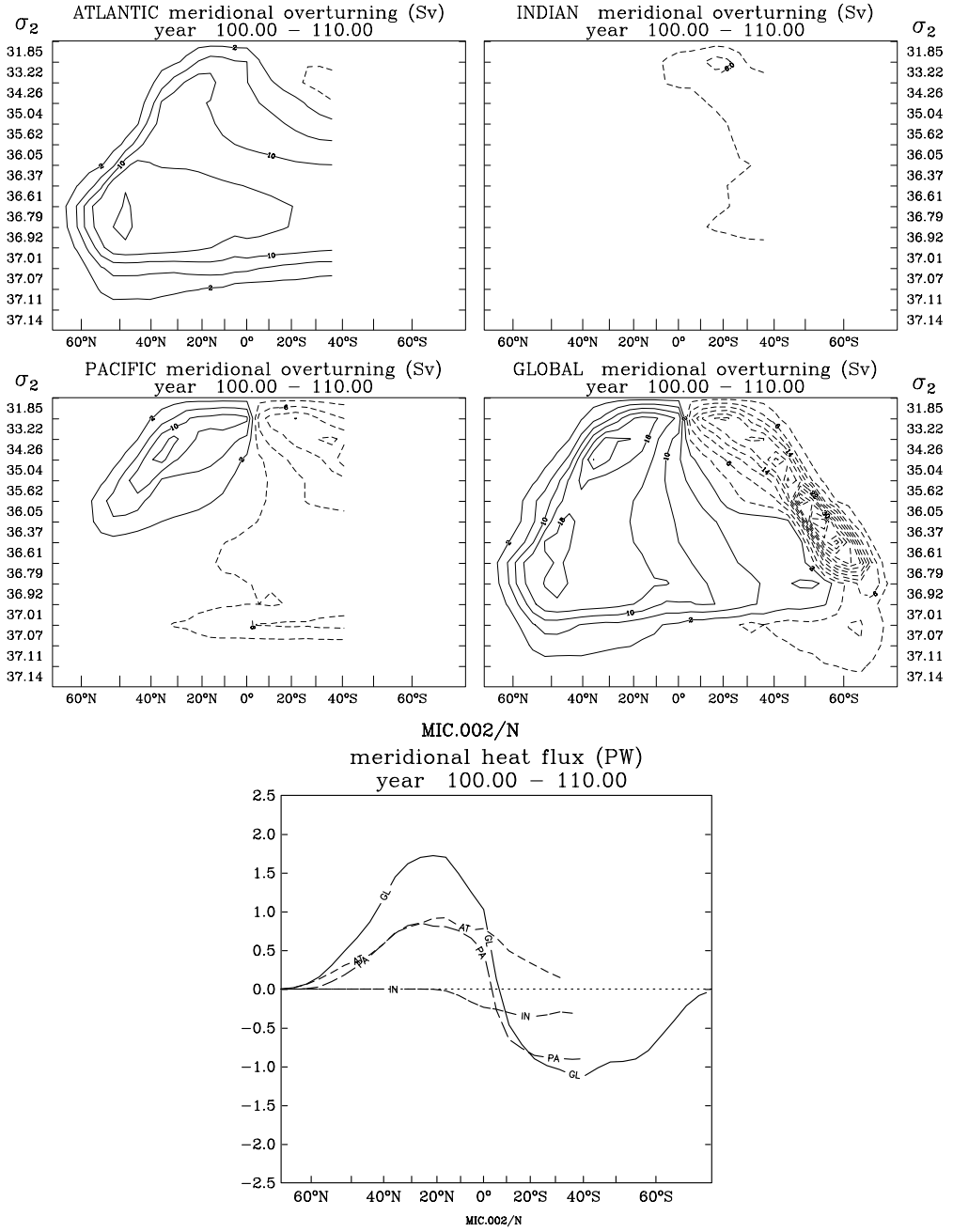

Fig. 5. Top 4 panels: meridional overturning streamfunction (Sv) in the 3 major basins and the world ocean from MICOM. Bottom: meridional heat flux (PW) in the 3 major basins (AT, IN, PA) and the world ocean (GL).

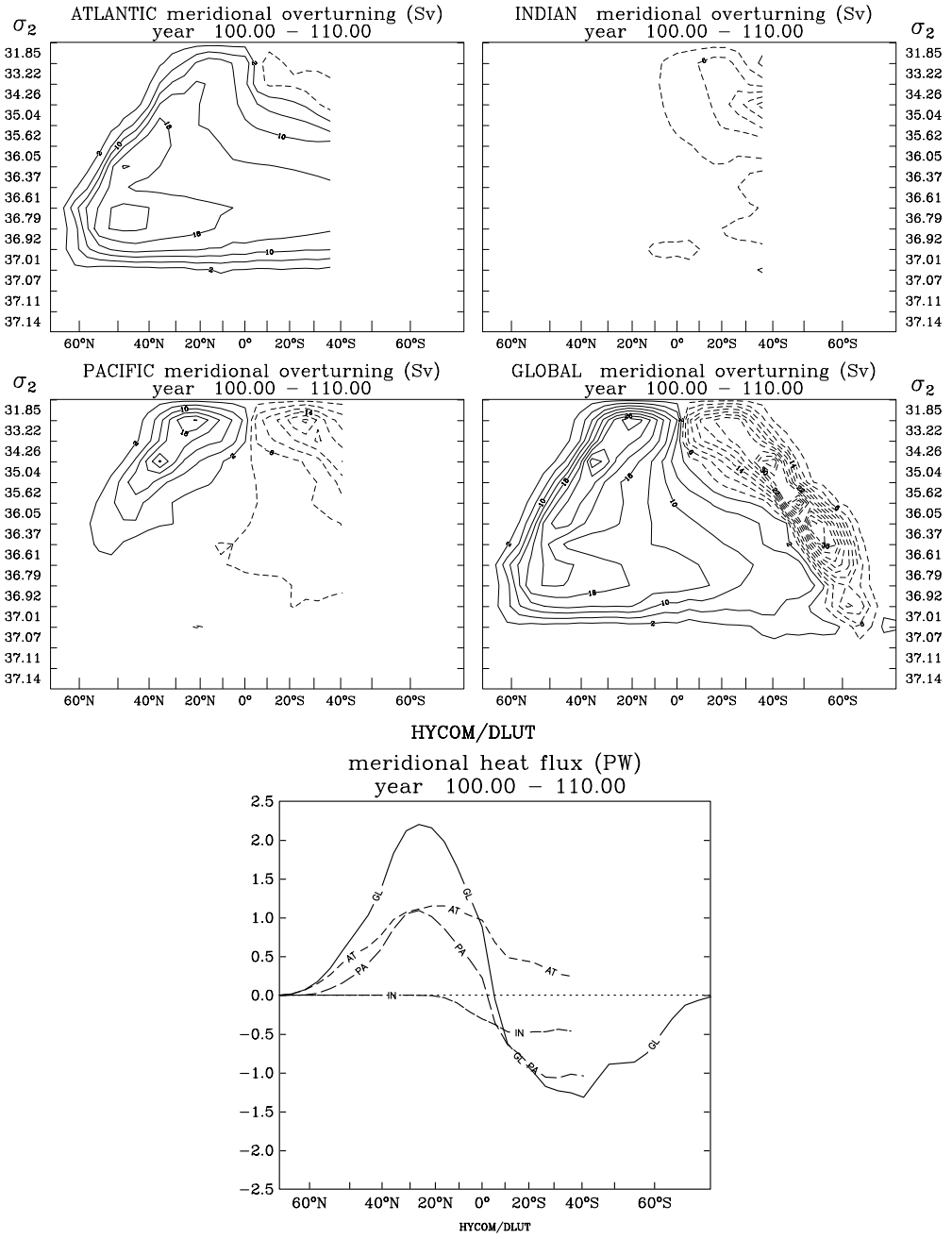

Fig. 6. As in Fig. 5, but for TS/DL run.

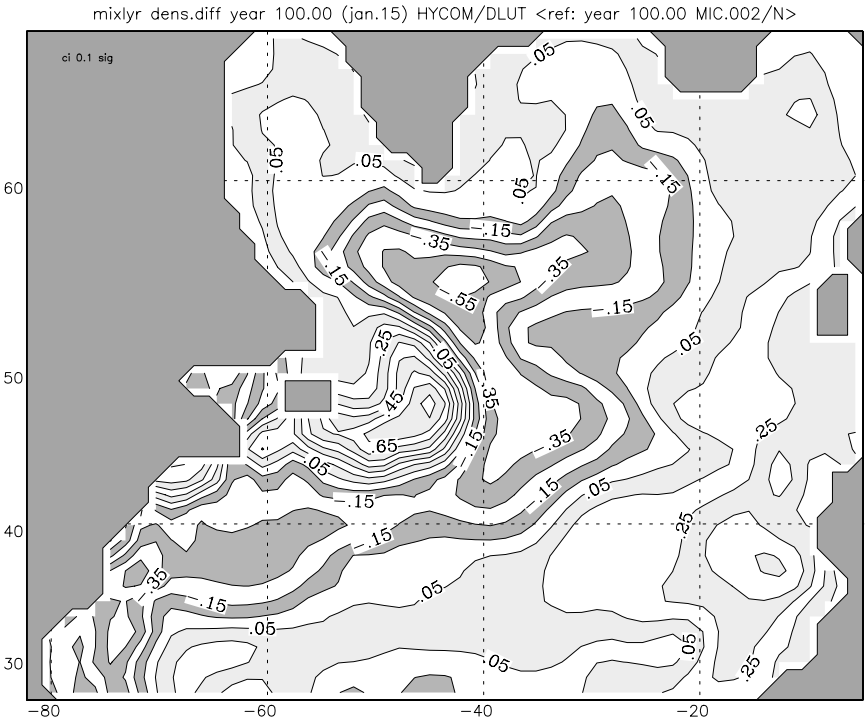

Fig. 7. North Atlantic surface density difference (σ_2 units) between TS/DL and MICOM run at year 100. Latitude/longitude marked at left/bottom.

(Fig. 10). Note the substantial downward mass flux (11 Sv) into layer 12 in the Labrador Sea in the RHO/DL simulation, one of many indicators that the RHO version of HYCOM bears closer resemblance to MICOM than does the TS version.

The similarities between Figs. 8 and 10 are no accident and come at a price. Both MICOM and HYCOMs RHO version achieve their relatively clean separation of 3-D mass fluxes into isopycnal and diapycnal components by emphasizing conservation of ρ_{pot} at the expense of conserving T. Unfortunately, this strategy eliminates not only numerically-induced cabbeling – that is, cabbeling caused by mutual inconsistencies in T, S *advection* –, but also "physical" cabbeling related to isopycnal *diffusion*. The relative importance of explicit T, S conservation achieved in the TS version of HYCOM and the clarity of the model's rendering of the thermohaline-forced circulation is an issue whose resolution will undoubtedly depend on the specific model application.

One measure of success of an oceanic circulation model is its ability to portray the equatorial current system. The performance of HYCOM in this regard is illustrated in Fig. 11 where meridional cross-equatorial sections through the upper 300 m of the water column from the TS/DL and RHO/UX runs are displayed together with the corresponding section from MICOM. As in Fig. 1, some liberty has been taken in drawing contour lines; fields that are piecewise constant in one coordinate direction (the vertical in this case) are difficult to display in black-and-white line graphics mode.

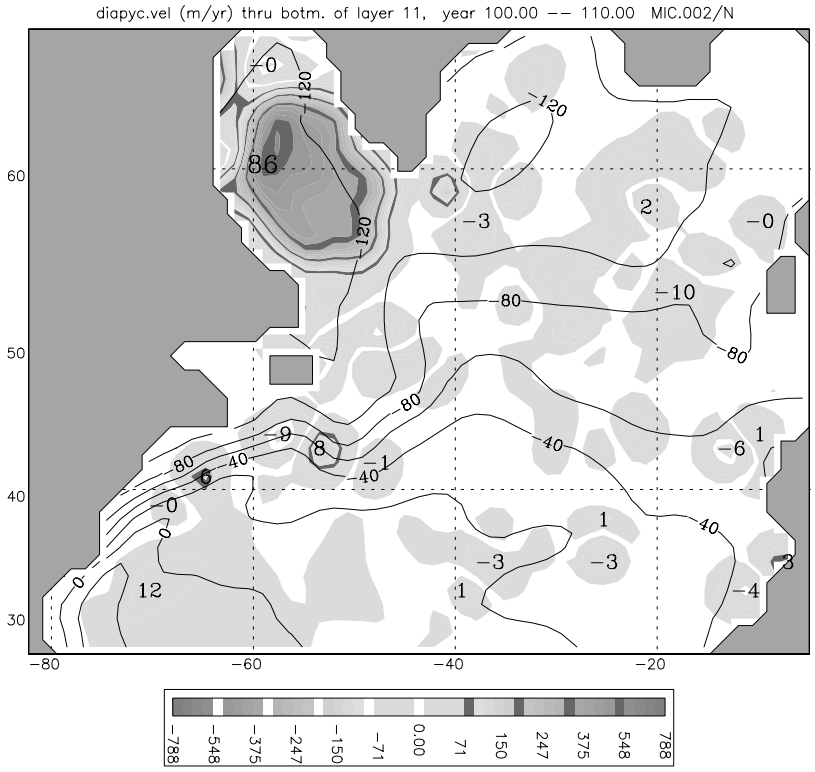

Fig. 8. Diapycnal flux through bottom of layer 11 in MICOM run. Grey-shaded contours: diapycnal vertical velocity (m/yr), positive downward. Solitary, variable-size numbers: regionally integrated diapycnal transport (0.1 Sv). Unshaded contour lines: mean sea surface height (cm). Latitude/longitude marked at left/bottom.

The feature of interest is the equatorial undercurrent, i.e., the closed set of isotachs centered on the equator at 150 m depth. The undercurrent has a surprisingly similar appearance in the three cross-sections, but fairly large differences are found in the strength of the equatorial surface flow. The high equatorial surface flow speed generated by MICOM, associated with a somewhat excessive equatorial SST minimum (note the strong doming of layer interfaces just below the surface in the MICOM solution), has been a long-standing concern. Specific reasons for this behavior have not been isolated. Layer interface displacements and flow speeds in the HYCOM solutions in Fig. 11 create the impression of higher implicit diffusion in HYCOM compared to MICOM. Qualitatively, this difference is in accord with the notion that HYCOM behaves like a fixed-grid model at shallow depths.

6. Concluding remarks

An attempt is made to combine, within a single model framework, certain features found in fixed-grid and isopycnic coordinate ocean circulation models that are usually considered mutually exclusive, namely, maintenance of vertical grid resolution regardless of stratification on the one

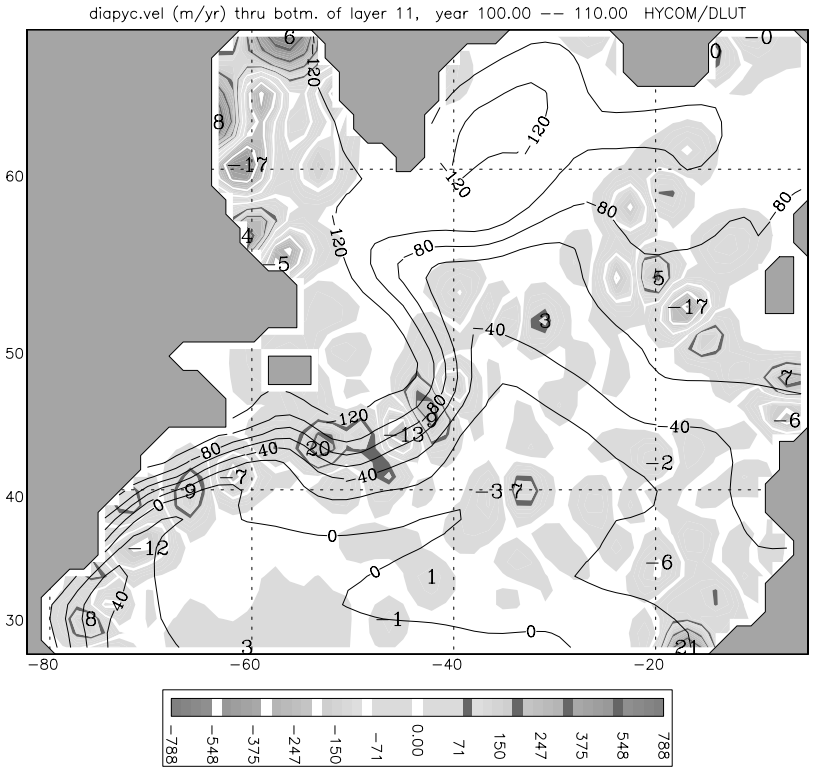

Fig. 9. Diapycnal flux through bottom of layer 11 in TS/DL run. See Fig. 8 for details.

hand, and alignment of coordinate surfaces with isopycnals on the other. Emphasis in this article is on technical documentation, but results from a few tests are presented that address the model's numerical and physical resilience.

The most unconventional, perhaps even discomforting aspect of the present model is the lack of a concise definition of the vertical coordinate. HYCOM grid points are free to move up and down in the water column, subject only to the "mandate" to maximize isopycnal coordinate representation in the model domain while at the same time avoiding formation of massless layers near the sea surface. It is unlikely that a closed formula exists that can match the present algorithm in its ability to optimize the effect of these two constraints in a noninterfering manner.

The "discomfort" most likely will be with us for some time, and since there is no formal assurance or proof of uniform and predictable model behavior in situations ranging from typical to extreme – the type of assurance taken for granted, for example, in the case of scaled-depth (σ) coordinates popular in coastal and atmospheric models –, the best course of action for the time being is to put the model through an extensive series of practical tests. The results presented here should be viewed as a first round of such tests.

At the core of HYCOM is the so-called grid generator, an algorithm which moves grid points vertically through the fluid if it senses opportunities for improving isopycnal alignment of coordinate surfaces, or sees the need to restore their minimum separation. While the particular grid

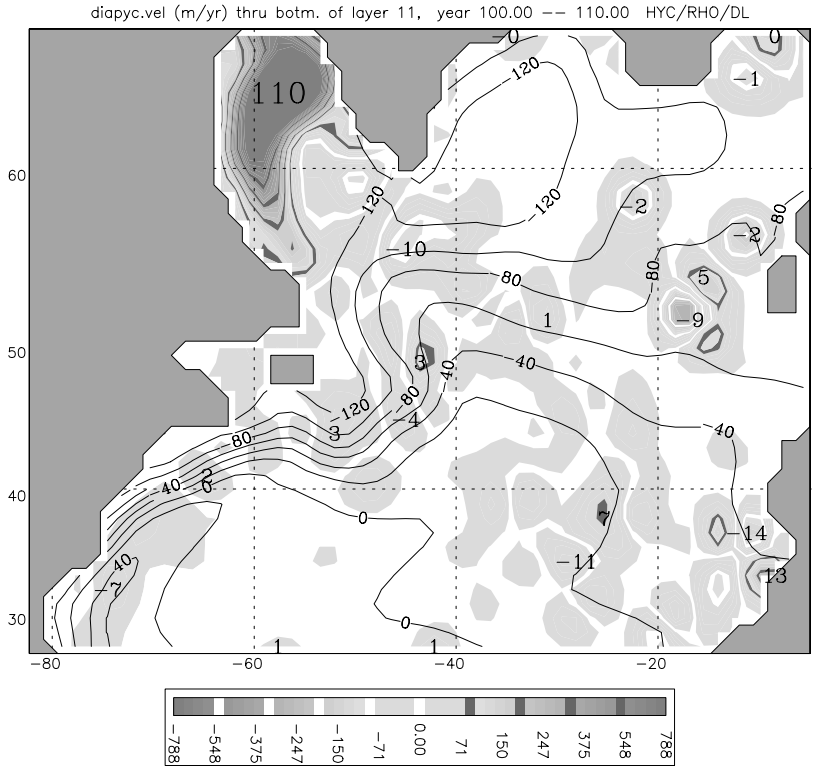

Fig. 10. Diapycnal flux through bottom of layer 11 in RHO/DL run. See Fig. 8 for details.

generator tested here appears to produce acceptable results in a broad sense, it should not be taken as the final word with regard to both coordinate surface placement and handling of the vertical advection terms resulting from nonmaterial movement of grid points. Our ultimate goal is to provide the user with a set of algorithmic and parametric grid generator options, and to encourage independent experimentation.

Substantially more work is also needed (i) to determine the model's sensitivity to the minimum layer thickness parameter δ used in the grid generator, and (ii) to develop strategies for finding the optimal number of low-density model layers. A large δ combined with too many model layers assigned to low target densities (i.e., to the warm water sphere) increases the likelihood that the Cartesian portion of the model domain will encroach upon the stratified region below the mixed layer where isopycnal coordinate representation clearly is desirable. The opposite extreme, a very small δ combined with too few low-density layers, is likely to degrade modeling of surface mixed layer processes. Investigation of the various tradeoffs sketched here has barely begun.

The present article totally sidesteps the question of how modern mixed layer closure schemes fare in a hybrid coordinate environment. The guaranteed presence of nicely separated coordinate surfaces in the oceanic surface layer invites replacement of MICOMs Kraus–Turner bulk mixed layer scheme by one based on second-order closure (K theory) or even higher order closure schemes. Experience with K theory schemes will be described in subsequent articles.

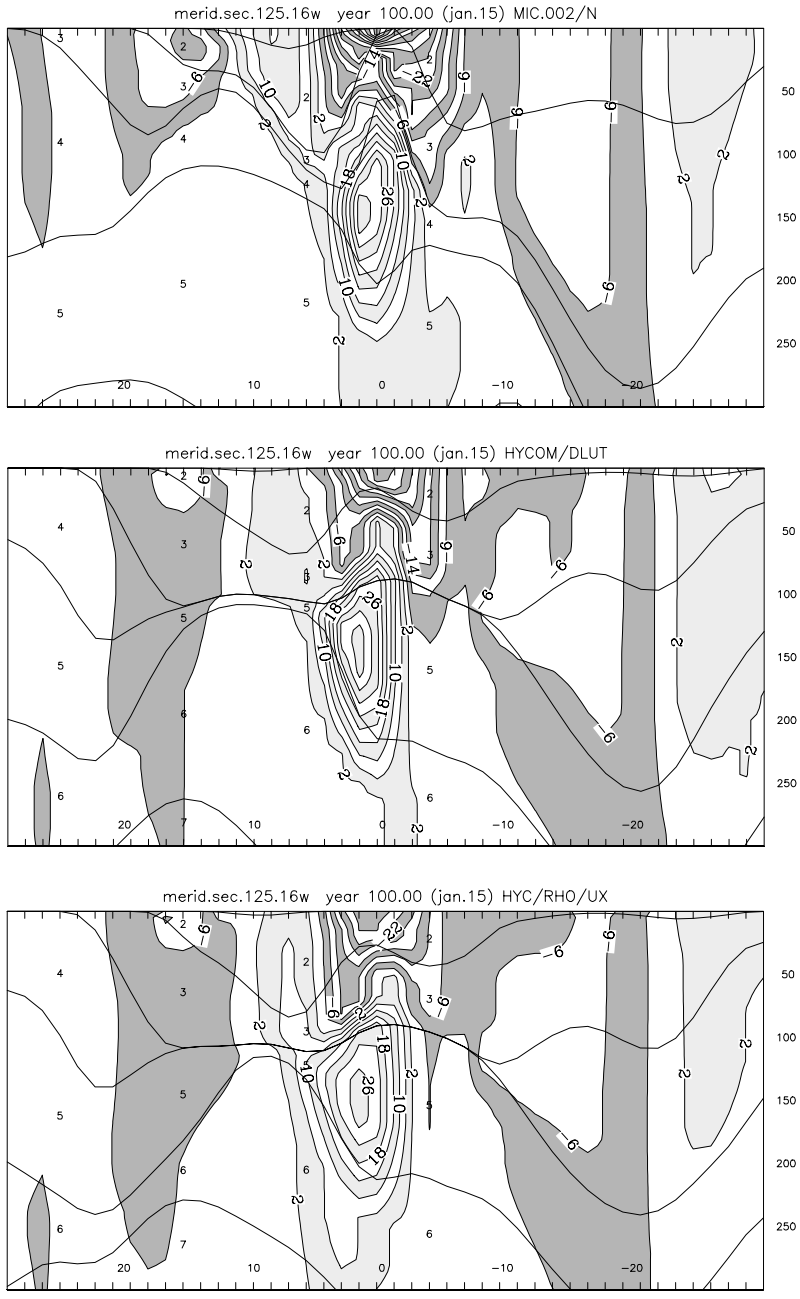

Fig. 11. Cross-equatorial section through uppermost 300 m of MICOM (top), TS/DL (middle), and RHO/UX solution (bottom) near 125°W. Shaded contours: zonal velocity (contour interval: 10 cm/s). Depth marked at right, latitude along bottom. Layers marked $3, 4, 5, \ldots$ correspond to model layers $1, 2, 3, \ldots$ given in Table 1. Layers marked 1 and 2, assigned densities 27.79 and 30.07, respectively, were added during postprocessing (see Appendix D) to assure correct rendering of low density water.

Acknowledgements

HYCOM development has been supported over the course of several years by the Office of Naval Research under Grant No. N00014-97-1-0096, by the US Dept. of Energy under Grant No. DE-FG02-98ER62608, and by a grant from the National Oceanic Partnership Program entitled "HYCOM Consortium for Data-Assimilative Ocean Modeling". For several years, this work has benefitted from interactions with a team of oceanographers and computer scientists, some of whose efforts and accomplishments in this context are highlighted at the web site http://hycom.rsmas.miami.edu. The author in particular wishes to recognize his coworkers Shan Sun, Linda Smith, George Halliwell, Eric Chassignet, and Alan Wallcraft.

Appendix A. Formulation of the horizontal pressure gradient force (PGF) in generalized coordinates

Both MICOM and HYCOM solve the horizontal momentum equations in advective form. Care must be exercised in this case to retain certain conservation properties inherent in the flux form of the equations.

In a hydrostatic fluid ($\partial\phi/\partial s = -\alpha\partial p/\partial s$), the layer-mass weighted horizontal PGF can be expressed as

$$\frac{\partial p}{\partial s}[\alpha\nabla_s p + \nabla_s\phi] = \nabla_s\left(\frac{\partial p}{\partial s}\alpha p\right) + \frac{\partial}{\partial s}(p\nabla_s\phi). \tag{A.1}$$

The form on the right-hand side of (A.1) has well-known implications for vortex spinup/spindown. Specifically, given that the curl of this expression is

$$\frac{\partial}{\partial s}(\nabla_s \times p\nabla_s\phi),$$

we can state that interface pressure torques governing vortex spinup/spindown in individual s coordinate layers have the form $(\nabla_s \times p\nabla_s\phi)$.

Orderly transmission of pressure torques up and down the water column is important for maintaining Sverdrup balance. The task before us, therefore, is to find a finite-difference expression for the PGF term $[\alpha\nabla_s p + \nabla_s\phi]$ in the horizontal momentum equation that can, after multiplication by layer thickness, be transformed by finite-difference operations into a finite-difference analog of the right-hand side of (A.1).

We start by writing the x component of the last term in (A.1) in the simplest possible – and hence noncontroversial – form $\delta_s(\overline{p}^x\delta_x\phi)$, where the δ and overbar operators denote 2-point centered differentiation and interpolation (averaging), respectively. Finite-difference product differentiation rules allow this expression to be expanded as follows:

$$\begin{aligned}\delta_s(\overline{p}^x\delta_x\phi) &= (\delta_s\overline{p}^x)\delta_x\overline{\phi}^s + \overline{p}^{xs}\delta_x\delta_s\phi \\ &= (\delta_s\overline{p}^x)\delta_x\overline{\phi}^s - \overline{p}^{xs}\delta_x(\alpha\delta_s p) \\ &= (\delta_s\overline{p}^x)\delta_x\overline{\phi}^s - \delta_x(\overline{p}^s\alpha\delta_s p) + \overline{\alpha\delta_s p}^x\delta_x\overline{p}^s.\end{aligned}$$

A finite-difference equation matching (A.1) is now obtained by rearranging terms and adding an analogous expression for the y component:

$$\overline{\alpha\delta_s p}^{x}\,\delta_x\overline{p}^{s} + (\delta_s\overline{p}^{x})\delta_x\overline{\phi}^{s} = \delta_x(\overline{p}^{s}\alpha\delta_s p) + \delta_s(\overline{p}^{x}\delta_x\phi),$$
$$\overline{\alpha\delta_s p}^{y}\,\delta_y\overline{p}^{s} + (\delta_s\overline{p}^{y})\delta_y\overline{\phi}^{s} = \delta_y(\overline{p}^{s}\alpha\delta_s p) + \delta_s(\overline{p}^{y}\delta_y\phi).$$

The last two equations state that, in order to preserve the conservation properties expressed by (A.1), the finite-difference PGF must be evaluated in the form

$$\alpha\nabla_s p + \nabla_s\phi = \begin{pmatrix} \dfrac{\overline{\alpha\delta_s p}^{x}}{\overline{\delta_s p}^{x}}\,\delta_x\overline{p}^{s} + \delta_x\overline{\phi}^{s} \\[2ex] \dfrac{\overline{\alpha\delta_s p}^{y}}{\overline{\delta_s p}^{y}}\,\delta_y\overline{p}^{s} + \delta_y\overline{\phi}^{s} \end{pmatrix}. \tag{A.2}$$

The salient result of the above analysis is that writing the undifferentiated factor α in the PGF formula as simply $\overline{\alpha}^{x}$ or $\overline{\alpha}^{y}$ can lead to spurious momentum and vorticity generation. To avoid this pitfall, α must appear in the PGF formula in layer thickness-weighted form.

For use in isopycnal or quasi-isopycnal models, it is convenient to express the PGF in terms of the Montgomery potential $M = \phi + p\alpha$. The proper finite-difference analog of M in a staggered vertical grid (p and ϕ carried on layer interfaces, α carried within a layer) is

$$M = \overline{\phi}^{s} + \alpha\overline{p}^{s},$$

which can easily be shown to be consistent with the two common forms of the hydrostatic equation,

$$\delta_s\phi = -\alpha\delta_s p, \quad \delta_s M = p\delta_s\alpha.$$

(These are finite-difference analogs of $\partial\phi/\partial p = -\alpha$ and $\partial M/\partial\alpha = p$, respectively.)

We begin the task of converting (A.2) into a form involving M by writing the x component of (A.2) as

$$\frac{\overline{\alpha\delta_s p}^{x}}{\overline{\delta_s p}^{x}}\,\delta_x\overline{p}^{s} + \delta_x\overline{\phi}^{s} = \delta_x M + \left[\frac{\overline{\alpha\delta_s p}^{x}}{\overline{\delta_s p}^{x}}\,\delta_x\overline{p}^{s} - \delta_x(\alpha\overline{p}^{s})\right]. \tag{A.3}$$

Making use of the relation

$$\overline{AB}^{x} - \overline{A}^{x}\overline{B}^{x} = \frac{1}{4}(\delta'_x A)(\delta'_x B),$$

where δ'_x represents the difference between two neighboring grid points, i.e., $\delta'_x = \Delta x\delta_x$, the term in square brackets in (A.3) can be expanded into

$$\begin{aligned}\frac{1}{\overline{\delta_s p}^{x}}\left(\overline{\alpha\delta_s p}^{x} - \overline{\alpha}^{x}\overline{\delta_s p}^{x}\right)\delta_x\overline{p}^{s} - \overline{p}^{sx}\delta_x\alpha &= \frac{1}{4\overline{\delta_s p}^{x}}(\delta'_x\delta_s p)(\delta'_x\alpha)\delta_x\overline{p}^{s} - \overline{p}^{sx}\delta_x\alpha \\ &= \frac{1}{4\overline{\delta_s p}^{x}}\left[(\delta'_x\delta_s p)(\delta'_x\overline{p}^{s}) - 4\overline{p}^{sx}\delta_s\overline{p}^{x}\right]\delta_x\alpha.\end{aligned}$$

The above expression involves a total of four p points, located one grid distance Δx apart on two consecutive s surfaces. Substantial simplification of this expression is possible by labeling the four points as

$$p_1 = p\left(x - \frac{\Delta x}{2}, s - \frac{\Delta s}{2}\right), \quad p_2 = p\left(x + \frac{\Delta x}{2}, s - \frac{\Delta s}{2}\right),$$
$$p_3 = p\left(x - \frac{\Delta x}{2}, s + \frac{\Delta s}{2}\right), \quad p_4 = p\left(x + \frac{\Delta x}{2}, s + \frac{\Delta s}{2}\right).$$

With a modest amount of arithmetic, it can now be shown that the term in square brackets in (A.3) reduces to

$$\frac{p_1 p_2 - p_3 p_4}{(p_4 - p_2) + (p_3 - p_1)} \delta_x \alpha.$$

This term, which in combination with the term $\delta_x M$ gives the PGF in x direction, is the sought-after finite-difference analog of $-p\partial\alpha/\partial x$ in

$$\alpha \nabla_s p + \nabla_s \phi = \nabla_s M - p \nabla_s \alpha.$$

The finite-difference expression for the PGF in y direction is analogous.

Appendix B. Vertical heat flux calculation in the presence of ice

In the simple "energy loan" ice model, the ice surface temperature calculation is based on the assumption that the system is energetically in a steady state, i.e., the heat flux through the ice matches the atmospheric heat flux. To illustrate this approach, we write the atmospheric heat flux as $F_{\text{air}} = a(T - T_{\text{a}})$, and the heat flux through the ice as $F_{\text{ice}} = b(T_{\text{w}} - T)$, where $T_{\text{a}}, T_{\text{w}}$ denote air and water temperature, respectively, while T is the ice surface temperature – the unknown in the problem. a, b are proportionality factors.

Given T_{a}, T_{w} and a first-guess value for T, we seek to modify T such that the difference between F_{ice} and F_{air} is eliminated, or at least reduced. The equation describing this situation is

$$a(T + \mathrm{d}T - T_{\text{a}}) = b(T_{\text{w}} - T - \mathrm{d}T),$$

which yields

$$\mathrm{d}T = \frac{aT_{\text{a}} + bT_{\text{w}}}{a + b} - T. \tag{B.1}$$

In order to make this formula applicable in situations where F_{air} is a mixture of sensible, latent, and radiative heat fluxes, we add $aT - aT$ and $bT - bT$ to the numerator of (B.1):

$$\mathrm{d}T = \frac{aT_{\text{a}} - aT + aT + bT_{\text{w}} - bT + bT}{a + b} - T.$$

After substituting the original definitions of $F_{\text{air}}, F_{\text{ice}}$, this expression reduces to the rather general formula

$$\mathrm{d}T = \frac{F_{\mathrm{ice}} - F_{\mathrm{air}}}{a + b}. \tag{B.2}$$

The new temperature $T + \mathrm{d}T$ must not be allowed to exceed 0 °C until the ice is melted completely.

Practical application of (B.2) requires knowledge of the coefficients a, b which represent the derivatives $\mathrm{d}F_{\mathrm{air}}/\mathrm{d}T$ and $\mathrm{d}F_{\mathrm{ice}}/\mathrm{d}T$, respectively. Guidance on the magnitude of a can be obtained from the conventional heat flux bulk formula. It suggests $a = c_{\mathrm{t}}\rho c_{\mathrm{p}}U$ where c_{t} is a nondimensional transfer coefficient (similar to the drag coefficient), ρ is the air density, c_{p} is the specific heat of air at constant pressure, and U is the wind speed. The formula for radiative energy loss, σT^4, suggests that the above estimate of a should be incremented by an amount of order $4\sigma T^3$. A reasonable choice for b is the ratio of ice thermal conductivity and ice thickness, $k_{\mathrm{ice}}/H_{\mathrm{ice}}$.

In the interest of computational efficiency in coupled climate models, we wish to minimize information exchange with the atmosphere. Toward this end, we make a independent of atmospheric state variables. To avoid oscillatory behavior in (B.2), a must be chosen somewhat larger than "typical" values of $c_{\mathrm{t}}\rho c_{\mathrm{p}}U + 4\sigma T^3$; in other words, we adopt a strategy of prudent underrelaxation of T.

Returning briefly to the energy loan concept, we finally need a statement relating the rate of energy borrowing or repaying to the composite atmospheric heat flux

$$F = cF_{\mathrm{ice}} + (1 - c)F_{\mathrm{opw}}, \tag{B.3}$$

where F_{opw} is the energy flux over open water and c is the fractional ice coverage.

We assume that F as defined in (B.3) is the energy flux felt by the ocean irrespective of the presence of ice. In other words, we assume that the energy flux between atmosphere and ice, F_{ice}, equals the energy flux between ice and ocean. This assumption is compatible with the steady state (zero heat flux divergence) assumption made in deriving (B.2).

Appendix C. A prototype grid generator

Consider three consecutive isopycnic layers, labeled 0, 1, 2, in a stratified water column. Let $\alpha_k > \alpha_{k+1}$, where α is the specific volume. Label the interfaces such that interface k denotes the *upper* interface of layer k.

Suppose α_1 differs from its layer reference value $\hat{\alpha}_1$. We seek ways to re-discretize the water column in a manner that preserves the overall height of the column, represented by the integral $\int \alpha \,\mathrm{d}p$, while changing α_1 to $\hat{\alpha}_1$. Conservation of the integral, which is important for preserving the geostrophic balance throughout the column, requires that alterations of α_1 must be accompanied by vertical displacement (in p space) of one or more interfaces. The simplest solution is to move only one interface and to select this interface in the spirit of the "donor cell" transport scheme. By this we mean that the upper interface is moved upward, i.e., layer 1 is diluted with lighter water from layer 0, if layer 1 is too dense ($\alpha_1 < \hat{\alpha}_1$). Analogously, the lower interface is moved downward, i.e., layer 1 is diluted with denser water from layer 2, if layer 1 is too light ($\alpha_1 > \hat{\alpha}_1$). This method of restoration does not work in the special case where the coordinate layer touching the sea floor is too light, and like all upstream advection schemes it is inherently diffusive. Methods

for conserving the integral $\int \alpha \, \mathrm{d}p$ by extruding water to a neighboring layer, rather than entraining water, will be discussed later.

Case 1 ($\alpha_1 < \hat{\alpha}_1$). This is the case where the *upper* interface is moved, i.e., mass is exchanged between layers 0 and 1. Conservation of $\int \alpha \, \mathrm{d}p$ requires

$$\alpha_0(p_1 - p_0) + \alpha_1(p_2 - p_1) = \alpha_0(\hat{p}_1 - p_0) + \hat{\alpha}_1(p_2 - \hat{p}_1), \tag{C.1}$$

where $\hat{p}_1$ is the pressure of the upper interface after re-discretization. Solving (C.1) for $\hat{p}_1$ yields the expression

$$\hat{p}_1 = \frac{p_1(\alpha_0 - \alpha_1) + p_2(\alpha_1 - \hat{\alpha}_1)}{\alpha_0 - \hat{\alpha}_1}. \tag{C.2}$$

Note that the weight assigned to p_2 is negative, indicating that for large discrepancies between α_1 and $\hat{\alpha}_1$ (C.2) will not necessarily yield a solution $\hat{p}_1 > p_0$. To assure a minimum interface spacing, we therefore replace $\hat{p}_1$ by

$$\tilde{p}_1 = \max(\hat{p}_1, p_0 + \Delta_0), \tag{C.3}$$

where Δ_0 is a minimum pressure difference. Moving the interface to $\tilde{p}_1$ instead of $\hat{p}_1$ means, of course, that layer 1 will end up with a specific volume $\tilde{\alpha}_1$ different from the reference value $\hat{\alpha}_1$.

Following BB81, Δ_0 is chosen to be a continuously differentiable function which for large positive arguments $\Delta p \equiv \hat{p}_1 - p_0$ returns the argument Δp (meaning that $\tilde{p}_1 = \hat{p}_1$), while for large negative arguments it returns a small constant δ representing the lowest permissible layer thickness. Our traditional choice for this so-called "cushion" function (Bleck and Benjamin, 1993) is

$$\Delta_0 = \begin{cases} \Delta p & \text{if } \dfrac{\Delta p}{\delta} > 4, \\ \delta\left[1 + \dfrac{1}{3}\left(\dfrac{\Delta p}{2\delta} + 1\right)^2\right] & \text{if } -2 < \dfrac{\Delta p}{\delta} < 4, \\ \delta & \text{if } -2 > \dfrac{\Delta p}{\delta}, \end{cases} \tag{C.4}$$

which is obtained by fitting a piece of a parabola in $(\Delta p, \Delta_0)$ space between the two straight lines $\Delta_0 = \Delta p$ and $\Delta_0 = \delta$. Another example from this class of spliced-together cushion functions, this one acting over a somewhat wider range of $\Delta p/\delta$, is

$$\Delta_0 = \begin{cases} \Delta p & \text{if } \dfrac{\Delta p}{\delta} > 6, \\ \delta\left[1 + \dfrac{4}{5}\left(\dfrac{\Delta p}{4\delta} + 1\right)^2\right] & \text{if } -4 < \dfrac{\Delta p}{\delta} < 6, \\ \delta & \text{if } -4 > \dfrac{\Delta p}{\delta}. \end{cases} \tag{C.5}$$

Note that the above cushion functions, whose purpose it is to smooth the transition between isopycnally and geometrically constrained segments of a coordinate surface, make no reference to neighboring grid points. This simplicity lends a degree of robustness to our hybrid scheme not necessarily found in more complicated formulas.

Two cases must be distinguished in computing $\tilde{\alpha}_1$ from (C.1):

Case 1a ($\tilde{p}_1 < p_1$). In this case, the interface ends up at a lower pressure, allowing lighter water to raise α_1 to a value $\tilde{\alpha}_1$ closer – if not equal – to the reference value $\hat{\alpha}_1$. The value $\tilde{\alpha}_1$ is obtained by substituting tildes for carats in (C.1):

$$\tilde{\alpha}_1 = \frac{\alpha_1(p_2 - p_1) + \alpha_0(p_1 - \tilde{p}_1)}{p_2 - \tilde{p}_1}. \tag{C.6}$$

Case 1b ($\tilde{p}_1 > p_1$). In this case, layer 1 "donates" water to layer 0; hence, it is α_0, rather than α_1, that is being modified. Conservation of $\int \alpha \, dp$ then leads to

$$\tilde{\alpha}_0 = \frac{\alpha_1(\tilde{p}_1 - p_0) + \alpha_0(p_1 - p_0)}{\tilde{p}_1 - p_0}. \tag{C.7}$$

Before solving (C.7), $\tilde{p}_1$ must be modified, if necessary, to satisfy $\tilde{p}_1 \leqslant p_2 - \Delta_2$, where Δ_2 is a layer thickness threshold presently set to $(p_2 - p_1)/2$.

Case 2 ($\alpha_1 > \hat{\alpha}_1$). This is the situation in which we decide to move the *lower* interface. The equation replacing (C.1) in this case is

$$\alpha_1(p_2 - p_1) + \alpha_2(p_3 - p_2) = \hat{\alpha}_1(\hat{p}_2 - p_1) + \alpha_2(p_3 - \hat{p}_2). \tag{C.8}$$

It calls for moving the pressure of the lower interface from p_2 to

$$\hat{p}_2 = \frac{p_1(\hat{\alpha}_1 - \alpha_1) + p_2(\alpha_1 - \alpha_2)}{\hat{\alpha}_1 - \alpha_2}. \tag{C.9}$$

The concern in this case is that $\hat{p}_2$ may get too close to, or even exceed, p_3. We therefore replace $\hat{p}_2$ by

$$\tilde{p}_2 = \min(\hat{p}_2, p_3 - \Delta_3) \tag{C.10}$$

with Δ_3 currently set to $(p_3 - p_2)/2$. Replacing $\hat{p}_2$ by $\tilde{p}_2$ in (C.8) changes $\hat{\alpha}_1$ into

$$\tilde{\alpha}_1 = \frac{\alpha_2(\tilde{p}_2 - p_2) + \alpha_1(p_2 - p_1)}{\tilde{p}_2 - p_1}. \tag{C.11}$$

Case 2a ($\alpha_1 > \hat{\alpha}_1$ *where layer* 1 *is the bottom layer*). Since the lower interface cannot move down in this case, we use (C.1) and compute an upper interface movement from (C.2). While it may sound physically implausible that the density in a layer can be manipulated by extruding water into an adjacent layer, this operation is legitimate if one conceptually allows density to vary vertically within a coordinate layer.

Specifically, as long as $\alpha_0 > \alpha_1 (> \hat{\alpha}_1)$, layer 1 may be viewed as being composed of two sublayers, one of specific volume α_0 and one of specific volume $\hat{\alpha}_1$. Having the same density as layer 0, the lighter sublayer can be merged with layer 0. The denser sublayer, which has the desired density $\hat{\alpha}_1$, stays in layer 1.

To keep $\hat{p}_1$ from exceeding the bottom pressure p_2, we replace $\hat{p}_1$ by

$$\tilde{p}_1 = \min(\hat{p}_1, p_2 - \Delta_2) \tag{C.12}$$

with Δ_2 currently set to $(p_2 - p_1)/2$.

The above algorithm for redistributing mass and density among model layers needs to be amended by a prescription for vertically redistributing thermodynamic variables *other* than mass and density. This is a particularly vexing issue for hybrid models carrying T, S (as opposed to α, S) as prognostic variables.

One possible approach is to translate $\hat{p}_k - p_k$ into a generalized vertical velocity (i.e., vertical motion relative to the layer interface) which is then used to advect T and S. Ideally, this vertical advection process should (i) conserve T, S in the column, and (ii) produce T, S changes in layer 1 that satisfy (C.1).

A scheme that exactly satisfies (i) while approximately satisfying (ii) can be obtained by reapportioning T, S among the layers in a manner analogous to (C.6), (C.7) and (C.11), whichever is applicable. In Case 1a, for example, where layer 1 properties are being modified by adding water from layer 0, this means

$$\tilde{T}_1 = \frac{T_1(p_2 - p_1) + T_0(p_1 - \tilde{p}_1)}{p_2 - \tilde{p}_1},$$
$$\tilde{S}_1 = \frac{S_1(p_2 - p_1) + S_0(p_1 - \tilde{p}_1)}{p_2 - \tilde{p}_1}.$$

The new values $\tilde{T}_1, \tilde{S}_1$ would combine to produce the desired specific volume $\tilde{\alpha}_1$ in layer 1 if the equation of state were linear, i.e., if

$$\tilde{\alpha}_1 - \alpha_1 = \left(\frac{\partial \alpha}{\partial T}\right)_S (\tilde{T}_1 - T_1) + \left(\frac{\partial \alpha}{\partial S}\right)_T (\tilde{S}_1 - S_1)$$

were exactly satisfied. This not being the case, the specific volume implied by $\tilde{T}_1, \tilde{S}_1$ will differ slightly from the prescribed value $\tilde{\alpha}_1$. In cases where $\tilde{\alpha}_1$ equals the layer reference value $\hat{\alpha}_1$, this difference prevents the scheme from exactly restoring isopycnic conditions in one instant. This disadvantage is likely to be inconsequential, however, because repetitive use of the coordinate restoration scheme presented here will quickly reduce the residual difference to zero.

Hybrid models carrying the pair α, S as prognostic variables while diagnosing T from the equation of state do not suffer from this particular complication, because α in such models is not affected by the process of redistributing S among layers. Note, however, that the curvature of isopycnals in T, S space is such that α, S-conserving models will see a small but systematic rise in $\int T \, \mathrm{d}p$ as a result of vertical remapping.

Division of a coordinate layer into two sublayers of differing densities and extruding one for the purpose of altering the layer's original density requires special consideration. The strategy presently adopted in Case 2a is to unmix T and S in a direction *perpendicular* to the isopycnal α_1 in T/S space. Details are as follows.

Define nondimensional temperature and salinity as $T' = T/T_{\mathrm{scl}}$ and $S' = S/S_{\mathrm{scl}}$. Setting the left-hand side in the expression

$$\mathrm{d}\alpha = \frac{\partial \alpha}{\partial T'} \mathrm{d}T' + \frac{\partial \alpha}{\partial S'} \mathrm{d}S'$$

to zero reveals that the vector $(\mathrm{d}T', \mathrm{d}S')$ pointing in the direction *tangential* to an isopycnal in T/S space must be perpendicular to the vector $(\partial\alpha/\partial T', \partial\alpha/\partial S')$. Hence, the direction *normal* to the isopycnal is perpendicular to the vector $(\partial\alpha/\partial S', -\partial\alpha/\partial T')$. This can be stated in the form

$$\frac{\mathrm{d}S'}{\partial\alpha/\partial S'} = \frac{\mathrm{d}T'}{\partial\alpha/\partial T'}.$$

Combining the last two expressions, we find that the increments $(\mathrm{d}T', \mathrm{d}S')$ changing the specific volume α to $\alpha + \mathrm{d}\alpha$ in a direction perpendicular to the isopycnal α are given by

$$\mathrm{d}T' = \mathrm{d}\alpha \frac{\partial\alpha/\partial T'}{(\partial\alpha/\partial T')^2 + (\partial\alpha/\partial S')^2}, \tag{C.13}$$

$$\mathrm{d}S' = \mathrm{d}\alpha \frac{\partial\alpha/\partial S'}{(\partial\alpha/\partial T')^2 + (\partial\alpha/\partial S')^2}. \tag{C.14}$$

Defining T, S in the two sublayers in Case 2a is now simply a matter of defining $\mathrm{d}\alpha$ in (C.13) and (C.14). To set the T/S properties in the lower sublayer, we set $\mathrm{d}\alpha = \hat{\alpha}_1 - \alpha_1$ while in the upper sublayer we set $\mathrm{d}\alpha = \alpha_0 - \alpha_1$.

Note that "perpendicularity" in T/S space depends on the scaling values $T_{\mathrm{scl}}, S_{\mathrm{scl}}$. The relative contribution of T and S unmixing to the creation of the required density contrast between the sublayers can be controlled by these scaling values. For example, as $T_{\mathrm{scl}}/S_{\mathrm{scl}} \to \infty$, density contrast is achieved entirely by T unmixing.

With the exception of Case 2a, the density restoration method outlined above may be viewed as an upstream or donor cell advection scheme whose diffusive character is a possible concern. Schemes that modify the density of both the receiving and the donating layer (an attribute found in the less diffusive centered-differencing schemes) offer a way to reduce this numerical diffusion. The density restoration scheme sketched below attempts to mimic the diffusion properties of centered differencing in a manner similar to the approach taken in Case 2a. Specifically, this scheme divides layer 1 into two sublayers, one of which has the desired target density $\hat{\alpha}_1$. The second sublayer is then expelled into either the layer above or below, depending on whether the second sublayer is lighter or denser than the first one.

Of utmost importance in the design of such an "unmixing" scheme is that it should not create artificial T, S extrema in the water column. To guarantee this, we require the unmixing process to be confined to a "bounding box" in T/S space whose four sides are defined in terms of T, S values in layers 0 and 2. Since the purpose of unmixing is to create sublayers of prescribed density, one or two corners of the bounding box may in practice be truncated by isopycnals representing the target densities of the two sublayers.

The sublayer generation routine presently in use treats the target density and T, S constraints as independent and requires that both be satisfied. The scheme tests two "candidate" unmixing directions as to their ability to create sublayers of the desired densities. Both unmixing directions are defined as lines that connect the T, S point representing the original layer 1 in T/S space with either the upper left or lower right corner of the bounding box. In either case, the unmixing line terminates on both ends on either the target isopycnal or the edge of the bounding box, whichever is encountered first. The unmixing direction ultimately chosen is the one that results in the bigger density contrast. Knowing the end points of the unmixing line, we can compute the thickness of the two sublayers by requiring T, S conservation during unmixing.

Examples of unmixing scenarios are shown in Fig. 12. Abscissa and ordinate in the three plots are salinity and temperature, respectively. The bounding box is dashed while the slanting curves

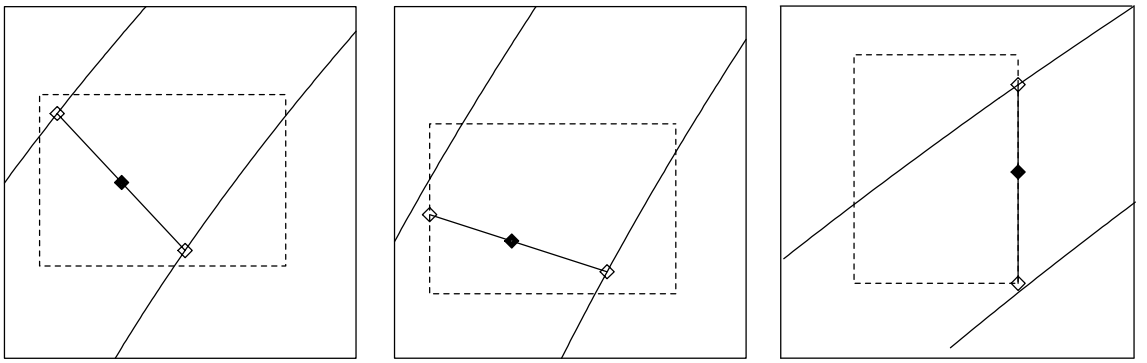

Fig. 12. Three examples of layer unmixing constrained by T/S bounding boxes (dashed) and bounding isopycnals (gently curved lines). Filled and hollow diamonds mark the T/S values before and after unmixing, respectively.

represent isopycnals. The black diamond represents the layer to be unmixed, while the hollow diamonds represent the two resulting sublayers.

Aside from reducing numerical diffusion, this unmixing scheme removes an undesirable bias from the coordinate restoration logic, namely, that layers subject to density restoration invariably *grow* at the expense of their neighbors. The present unmixing scheme has the opposite effect, i.e., it causes layers whose density is being manipulated to *shrink*. We use the cushion function described earlier to prevent a layer from getting too thin in the process. Our present strategy is to attempt partial coordinate restoration through unmixing before resorting to the donor cell method described earlier. The exact meaning of the word "partial" remains to be determined.

Since the grid generator consumes little time compared to other parts of HYCOM, timing tests fail to show a systematic impact of the unmixing scheme on model performance.

In the present grid generator implementation, the parameter δ appearing in (C.4) and (C.5) is set to 10 m. Except in very shallow water, it is advisable to make δ a constant. This will prevent the potential-vorticity conserving advection and Coriolis terms in the momentum equations, which are written in a shallow-water form inherited from MICOM, from generating spurious dynamic stretching effects. Keeping coordinate surfaces horizontal in geographic regions where layers are unable to retain their isopycnal character, i.e., where coordinate surfaces are not material under adiabatic flow conditions, assures that layer thickness drops out of the momentum advection and Coriolis terms, allowing them to act as they would in Cartesian coordinate models.

In shallow coastal areas, on the other hand, it is appropriate to scale δ by the total water depth. The argument here is that Taylor columns in the coastal zone are likely to span the whole water depth, implying that undulations in the depth of σ surfaces ($\sigma =$ depth scaled by bottom depth) accurately portray the stretching effect due to sea floor undulations.

Appendix D. Transformation of nonisopycnic model output to isopycnic coordinates

Let $\rho(p)$ be a piecewise constant (i.e., stairstep) density profile where the height Δp of each stairstep ("riser") represents the thickness of an isopycnic layer while the width $\Delta\rho$ of each stairstep represents the density increment between consecutive isopycnic layers. Both step widths

and riser heights are arbitrary. Our task is to transform this profile into another stairstep profile differing from the original one in that the location of the risers on the density axis is prescribed. The transformation should preserve the mean density in the column, i.e., the integral $\int \rho \, \mathrm{d}p$ taken from the sea surface to the bottom.

Let ρ_k ($k = 1, \ldots, n$, $\rho_{k+1} > \rho_k$) mark the points on the density axis where we want the new risers to be placed. We require that the ρ_k span the density range of the input profile, and that the input profile be monotonic. Denoting the height of the upper and lower interface bounding the kth layer by $p_{k-1/2}$ and $p_{k+1/2}$, respectively, the condition we wish to satisfy can then be stated as

$$\sum_{k=1}^{n} \rho_k (p_{k+1/2} - p_{k-1/2}) = \int_{p_{1/2}}^{p_{n+1/2}} \rho \, \mathrm{d}p. \tag{D.1}$$

The interface depths are the unknowns in the problem.

Integration of (D.1) by parts – on the left this amounts to reordering the terms under the summation sign – allows us to rewrite (D.1) as

$$\rho_n p_{n+1/2} - \rho_1 p_{1/2} - \sum_{k=1}^{n-1} p_{k+1/2} (\rho_{k+1} - \rho_k) = [\rho p]_{p_{1/2}}^{p_{n+1/2}} - \int_{\rho(p_{1/2})}^{\rho(p_{n+1/2})} p \, \mathrm{d}\rho.$$

By virtue of $\rho(p_{1/2}) \geqslant \rho_1$ and $\rho(p_{n+1/2}) \leqslant \rho_n$, this expression reduces to

$$\sum_{k=1}^{n-1} p_{k+1/2} (\rho_{k+1} - \rho_k) = \int_{\rho_1}^{\rho_n} p \, \mathrm{d}\rho. \tag{D.2}$$

Our strategy is to satisfy (D.2) by breaking the integral into pieces taken over intervals (ρ_k, ρ_{k+1}) and conserving each integral individually. This immediately leads to

$$p_{k+1/2} = \frac{1}{\rho_{k+1} - \rho_k} \int_{\rho_k}^{\rho_{k+1}} p \, \mathrm{d}\rho \quad (k = 1, \ldots, n-1).$$

The procedure for transforming the density profile is illustrated in Fig. 13.

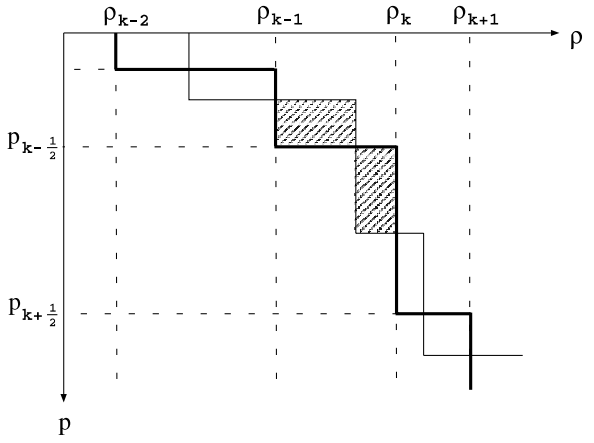

Fig. 13. Illustration of vertical transform procedure. Thin/thick stairstep lines represent input/output density profiles. Requiring the hatched areas to be of equal size yields location of $p_{k-1/2}$. See text for additional details.

Knowing the new interface depths, we can now proceed to transform other model output variables. Care must be exercised in transforming mass fluxes (that is, the product of velocity and layer thickness), because their vertical sum needs to be preserved if they are to be used for quantitative diagnostic work in density space. Note that preserving the vertical sum of mass fluxes is equivalent to preserving the vertical *integral* of the associated velocity field. Hence, if constraints patterned after (D.1) are used in transforming mass fluxes, the variable replacing ρ in (D.1) must be velocity, not mass flux.

In layer models like MICOM and HYCOM, where mass flux computation is a multi-step process involving a spatially varying mix of diffusive and antidiffusive fluxes, the first step in the flux transformation therefore is generation of an auxiliary velocity field representing mass flux divided by layer thickness. It is this velocity field that, after being transformed in a manner preserving its column integral, forms the basis for mass fluxes in ρ_k space.

References

Bleck, R., 1978a. Finite difference equations in generalized vertical coordinates. Part I: Total energy conservation. Contrib. Atmos. Phys. 51, 360–372.

Bleck, R., 1978b. On the use of hybrid coordinates in numerical weather prediction models. Mon. Weather Rev. 106, 1233–1244.

Bleck, R., 1984. An isentropic coordinate model suitable for lee cyclogenesis simulation. Riv. Meteorol. Aeronaut. 44, 189–194.

Bleck, R., 1998. Ocean modeling in isopycnic coordinates. In: Chassignet, E.P., Verron, J. (Eds.), Ocean Modeling and Parameterization, NATO Science Series. Kluwer Academic Publishers, Dordrecht, pp. 423–448.

Bleck, R., Benjamin, S.G., 1993. Regional weather prediction with a model combining terrain-following and isentropic coordinates. Part 1: Model description. Mon. Weather Rev. 121, 1770–1785.

Bleck, R., Boudra, D.B., 1981. Initial testing of a numerical ocean circulation model using a hybrid (quasi-isopycnic) vertical coordinate. J. Phys. Oceanogr. 11, 755–770.

Bleck, R., Boudra, D., 1986. Wind-driven spin-up in eddy-resolving ocean models formulated in isopycnic and isobaric coordinates. J. Geophys. Res. 91C, 7611–7621.

Bleck, R., Smith, L., 1990. A wind-driven isopycnic coordinate model of the north and equatorial Atlantic Ocean. 1. Model development and supporting experiments. J. Geophys. Res. 95C, 3273–3285.

Bleck, R., Rooth, C., Hu, D., Smith, L., 1992. Salinity-driven thermocline transients in a wind- and thermohaline-forced isopycnic coordinate model of the North Atlantic. J. Phys. Oceanogr. 22, 1486–1505.

Brydon, D., Sun, S., Bleck, R., 1999. A new approximation of the equation of state for sea water, suitable for numerical ocean models. J. Geophys. Res. 104, 1537–1540.

Drange, H., Bleck, R., 1997. Multidimensional forward-in-time upstream-in-space-based differencing for fluids. Mon. Weather Rev. 125, 616–630.

Gent, P.R., McWilliams, J.C., 1990. Isopycnal mixing in ocean circulation models. J. Phys. Oceanogr. 20, 150–155.

Hallberg, R., 2000. Time integration of diapycnal diffusion and Richardson number dependent mixing in isopycnal coordinate ocean models. Mon. Weather Rev., 1402–1419.

Higdon, R.L., Bennett, A.F., 1997. Barotropic–baroclinic time splitting for ocean circulation modeling. J. Comput. Phys. 135, 30–53.

Hirt, C.W., Amsden, A.A., Cook, J.L., 1974. An arbitrary Langrangian–Eulerian computing method for all flow speeds. J. Comput. Phys. 14, 227–253.

Janjic, Z., 1977. Pressure gradient force and advection scheme used for forecasting with steep and small scale topography. Contrib. Atmos. Phys. 50, 186–199.

Kasahara, A., 1974. Various vertical coordinate systems used for numerical weather prediction. Mon. Weather Rev. 102, 509–522.

Konor, C.S., Arakawa, A., 1997. Design of an atmospheric model based on a generalized vertical coordinate. Mon. Weather Rev. 125, 1649–1673.

Kraus, E.B., Turner, J.S., 1967. A one-dimensional model of the seasonal thermocline: II. The general theory and its consequences. Tellus 19, 98–106.

McDougall, T.J., Dewar, W.K., 1998. Vertical mixing and cabbeling in layered models. J. Phys. Oceanogr. 28, 1458–1480.

Montgomery, R.B., 1937. A suggested method for representing gradient flow in isentropic surfaces. Bull. Am. Meteorol. Soc. 18, 210–212.

Oberhuber, J.M., 1988. An Atlas Based on The 'COADS' Data Set: The Budgets of Heat, Buoyancy, and Turbulent Kinetic Energy At The Surface of The Global Ocean. Max-Planck-Institut für Meteorologie, Hamburg (ISSN 0937-1060).

Oberhuber, J.M., 1993. Simulation of the Atlantic circulation with a coupled sea ice-mixed layer-isopycnal general circulation model. Part I: Model description. J. Phys. Oceanogr. 23, 808–829.

Schmitz, W.J. Jr., 1996a. On the world ocean circulation: Vol. 1 – some global features/North Atlantic circulation. Woods Hole Oceanogr. Inst.,Tech. Rep. WHOI-96-03, Woods Hole, MA, 140 pp.

Schmitz, W.J. Jr., 1996b. On the world ocean circulation: Vol. 2 – the Pacific and Indian oceans/a global update. Woods Hole Oceanogr. Inst.,Tech. Rep. WHOI-96-08, Woods Hole, MA, 237 pp.

Schopf, P.S., Loughe, A., 1995. A reduced gravity isopycnal ocean model. Mon. Weather Rev. 123, 2839–2863.

Semtner Jr., A.J., 1976. A model for the thermodynamic growth of sea ice in numerical simulations of climate. J. Phys. Oceanogr. 6, 379–389.

Smagorinsky, J.S., 1963. General circulation experiments with the primitive equations. I: The basic experiment. Mon. Weather Rev. 91, 99–164.

Smith, L.T., 1992. Numerical simulations of stratified rotating flow over finite amplitude topography. J. Phys. Oceanogr. 22, 686–696.

Spencer, R.W., 1993. Global oceanic precipitation from the MSU during 1979–91 and comparisons to other climatologies. J. Climate 6, 1301–1326.

Starr, V.P., 1945. A quasi-Langrangian system of hydrodynamical equations. J. Meteorol. 2, 227–237.

Sun, S., Bleck, R., Rooth, C., Dukowicz, J., Chassignet, E., Killworth, P., 1999. Inclusion of thermobaricity in isopycnic-coordinate ocean models. J. Phys. Oceanogr. 29, 2719–2729.

Sun, S., Bleck, R., 2000. Thermohaline circulation studies with an isopycnic coordinate ocean model. J. Phys. Oceanogr. 31, 2761–2782.

Woodruff, S.D., Slutz, R.J., Jenne, R.L., Steurer, P.M., 1987. A comprehensive ocean-atmosphere data set. Bull. Am. Meteorol. Soc. 68, 1239–1250.

Zalesak, S., 1979. Fully multidimensional flux-corrected transport algorithms for fluids. J. Comput. Phys. 31, 335–362.

Zebiak, S.E., Cane, M.A., 1987. A model El Nino-Southern oscillation. Mon. Weather Rev. 115, 2262–2278.

Zhu, Z., Thuburn, J., Hoskins, B., Haynes, P., 1992. A vertical finite-difference scheme based on a hybrid sigma-theta-pressure coordinate. Mon. Weather Rev. 120, 851–862.